THESIS FOR THE DEGREE OF DOCTOR OF PHILOSOPHY

Characterization and Development of Packed-Fluidized Bed Reactors

NASRIN NEMATI

Department of Space, Earth and Environment

CHALMERS UNIVERSITY OF TECHNOLOGY

Gothenburg, Sweden 2024

Characterization and Development of Packed-Fluidized Bed Reactors
NASRIN NEMATI
ISBN 978-91-8103-099-0

Doktorsavhandlingar vid Chalmers tekniska högskola
Ny serie nr 5557
ISSN 0346-718X

Department of Space, Earth and Environment
Division of Energy Technology
Chalmers University of Technology
SE-412 58 Gothenburg
Sweden
Telephone + 46 (0)31-772 5213

Cover:
From left to right: Bubbling Fluidized Bed and Packed-Fluidized Bed. The zoomed-in section highlights a detailed view of the mass-transfer coefficients between particles in the emulsion phase and gas in the bubble phase.

Printed by: Chalmers Digitaltryck
Gothenburg, Sweden 2024

Characterization and Development of Packed-Fluidized Bed Reactors

NASRIN NEMATI
Division of Energy Technology
Department of Space, Earth and Environment
Chalmers University of Technology

Abstract

Packed- or confined fluidized beds utilize fixed packings inside a bed of fluidizing particles. This novel concept can have advantages with respect to gas-solid contact and solids flow patterns. This could be of importance for many fluidized bed conversion technologies, such as chemical-looping. In this thesis, different aspects of packed fluidized beds are explored, using experimental and modeling tools. The study includes an investigation of the effects of packings on heat and mass transfer, as well as solids flow patterns. For this purpose, different types of packings are selected and assessed.

Initially, the heat transfer coefficient to a horizontal tube submerged in a packed-fluidized bed, pressure drop, and vertical solids segregation are experimentally evaluated for bed temperatures ranging from 400°C to 900°C and superficial gas velocities from 0.04 m/s to 0.411 m/s. Subsequently, the conversion of gaseous fuels during CLC is investigated. CLC experiments are conducted using CH_4, CO, and syngas (50/50% H_2/CO) as fuels, at temperatures between 840°C and 940°C. Next, gas-solid mass transfer in a bubbling packed-fluidized bed is studied. This is achieved through targeted experiments using a bed of moist silica gel, where the rate of H_2O desorption is monitored during the experiments. A detailed mass transfer analysis is performed using a model that accounts for various steps in the mass transfer chain. Finally, the residence time distribution of bed material in a bubbling packed-fluidized bed with throughflow is examined. The cold-flow reactor setups allow for continuous cross-current and counter-current flow of particles and fluidizing gas. The effects of packing type, fluidization number, bed height, and solid throughflow rate are analyzed. The axial dispersion and tank-in-series models are utilized to categorize flow patterns of particles in packed-fluidized beds.

The results show that the nature of the packings have significant impact on the behavior of bubbling-fluidized beds. Packings with low void factor such as ASB have a lower heat transfer coefficient, higher pressure drop, and more significant vertical segregation, compared to a bubbling bed without packings. However, packings with high void factors such as RMSR showed an improvement in heat transfer coefficient (up to 1243 W/m^2K) at higher gas velocities compared to a bubbling bed with no packings (up to 1124 W/m^2K). Also, beds with RMSR and Hiflow packings had lower pressure drop, lower vertical segregation, and higher fuel conversion in CLC compared to a bubbling bed with no packings. Furthermore, the inhibition of bubble formation and growth in the packed-fluidized bed enhances the emulsion-bubble mass transfer by up to 23% compared to a bed without packings. As part of this work, it was also shown that low void factor packings can alter the mixing behavior of solids in BFBs. Without packings, the fluidizing solids are well mixed, similar to a continuous stirred tank reactor (CSTR), while packings could transmit the flow pattern to be more similar to a plug flow reactor (PFR). This was confirmed by the reactor modeling, with the tank-in-series model resulting in an increase in the number of reactors in series from 1 up to 10 reactors when using packings. Furthermore, the vessel dispersion number can be reduced up to tenfold in such packed-fluidized beds.

This work demonstrates that the use of packed-fluidized beds or confined fluidization has a significant effect on important phenomena in a bubbling fluidized bed. This could be of significance in a number of new and novel technologies, including chemical-looping combustion or gasification and hydrogen production systems.

Keywords: *Bubbling fluidized bed; Packed-fluidized bed; Confined fluidization; Random packing; Chemical-looping combustion; Mass transfer; Heat transfer; Residence Time Distribution.*

List of publications

The thesis is based on the following papers, which are referred to in the thesis by their Roman numerals:

I. Nemati N.; Andersson P.; Stenberg V.; Rydén M.; *Experimental investigation of the effect of random packings on heat transfer and particle segregation in packed-fluidized bed*. Industrial & Engineering Chemistry Research **2021**; https://doi.org/10.1021/acs.iecr.1c01221.

II. Nemati N.; Rydén M.; *Chemical-looping combustion in packed-fluidized beds: experiments with random packings in bubbling bed*. Fuel Processing Technology **2021**; https://doi.org/10.1016/j.fuproc.2021.106978.

III. Nemati N.; Tsuji Y.; Mattisson T.; Rydén M.; *Chemical-looping combustion in packed-fluidized bed reactor – fundamental modelling and batch experiments with random metal packings*. Energy & Fuels **2022**; https://doi.org/10.1021/acs.energyfuels.2c00527.

IV. Nemati N.; Moreno P. F.; Rydén M; *Investigation of the hydrodynamics of packed-fluidized beds: characterization of solids flux*. Fuel **2023**; https://doi.org/10.1016/j.fuel.2022.127010.

V. Nemati N.; Pallarès D.; Mattisson T.; Guío-Pérez D.C.; Rydén M.; *Experimental investigation and modeling of the impact of random packings on mass transfer in fluidized beds*. Powder Technology **2024**; https://doi.org/10.1016/j.powtec.2024.119781.

VI. Nemati N.; Pröll T.; Mattisson T.; Rydén M.; *Impact of random packing on residence time distribution of particles in bubbling fluidized beds: Part 1 - cross-current flow reactors*. Chemical Engineering Science **2024**; (under review).

VII. Nemati N.; Mattisson T.; Pallarès D; Guío-Pérez D.C.; Rydén M.; *Impact of random packing on residence time distribution of particles in bubbling fluidized beds: Part 2 - counter-current flow reactors*. Chemical Engineering Science **2024**; (submitted).

Contribution report

Paper I. Principal author, responsible for experimental work in M7-lab, supervision of experimental work, responsible for data evaluation and writing.

Paper II. Principal author, performed experimental work in M7-lab, data evaluation, and writing.

Paper III. Principal author, responsible for experimental work in M7-lab, supervision of experimental work, responsible for data evaluation, modeling, and writing.

Paper IV. Principal author, responsible for experimental work in M3-lab, supervision of experimental work, responsible for data evaluation and writing.

Paper V. Principal author, performed experimental work in M3 and chemistry labs, data evaluation, modeling, and writing.

Paper VI. Principal author, performed experimental work at BOKU University, data evaluation, modeling, and writing.

Paper VII. Principal author, performed experimental work in M3-lab, data evaluation, modeling, and writing.

Related publications not included in the thesis

- Nemati N.; Moreno P.F.; Rydén M.; *Investigation of the hydrodynamics of packed-fluidized beds: characterization of solids flux*. The 24th International Conference on Fluidized Bed Conversion, Göteborg, Sweden, **2022**.

- Nemati N.; Rydén M.; Mattisson T.; *Packed-fluidized-beds in chemical-looping combustion: the effect of random packing on synthesis gas conversion in bubbling bed*. The 6th International Conference on Chemical Looping, Zaragoza, Spain, **2022**.

- Nemati N.; Mattisson T.; Rydén M.; *Chemical-looping combustion in packed-fluidized bed reactor: Experimental and modeling investigation into the effect of random metal packings*. The 7th International Conference on Chemical Looping, Banff, Canada. **2024**.

Acknowledgments

my heartfelt gratitude to,

My supervisor Magnus Rydén and my co-supervisors Tobias Mattisson and David Pallarès for providing me the opportunity to pursue my PhD with your support. It has been a joy working with you all and thank you for all the help, discussions, and contributions to the work. Special thanks to Magnus, without whom I would not have dared to start this journey. You have always provided me with a pleasant environment to work in and have helped me anytime I needed it. I am profoundly grateful for your support whenever I saw an obstacle on the way of my PhD.

Tobias Pröll, Florian Pröll, Gerhard Hofer, David Wöß and everyone I had the pleasure of meeting and working with through my sabbatical at BOKU, thank you for your invaluable hospitality and willingness to share your knowledge and experience with me.

Swedish Energy Agency (projects 46525-1 - The application of confined fluidization in energy conversion, and P2022-00544 – production of hydrogen and biochar from wood fuels with a new process that utilizes the steam-iron reaction and iron ore concentrate), and Chalmerska forskningsfonden 2023 (90 211 102) are acknowledged for supporting my work, conferences, and sabbatical visit financially.

To my wonderful colleagues and friends in the CLC and fluidization groups, thank you for the engaging discussions, and for all the good teamwork and the joy of not working alone. All the fantastic inspirations that you gave me are greatly appreciated.

I have been privileged to have valued colleagues at two different divisions of Energy Technology, and Energy and Materials. It would not have been half the fun without you! It is clear that it is the supporting colleagues who make the working place such a good place to be. I have enjoyed all the discussions at fika, lunches, meetings, seminars, and when we cross paths at the corridors!

I also want to thank Rustan Hvitt, Marie Iwanow, Katarina Bergkvist, Jessica Malene Bohwalli, Johannes Öhlin, Ulf Stenman, and Anna Borg, for helping me untangle the endless knots in my head.

To my family—my mother, father, and sisters—you are my world. Thank you for your unconditional love, support, advice, and belief in me along the way. Andreas, your support on this journey and beyond has been more than I could ever ask for. Thank you for standing by my side through every challenge, and for being my greatest adventure!

This PhD journey has truly been the time of my life, so far...

Nasrin Nemati

Göteborg, June, 2024

List of symbols

A	s	area under the $c_{response}$ curve	k_f	$Nm^3kg^{-1}s^{-1}$	mass-based effective reaction contact factor
A_i	m^2	tube inner surface area	K_p	s^{-1}	transfer of h_2o from internal particle sites to the particle surface
A_o	m^2	tube outer surface area	k_r	$Nm^3kg^{-1}s^{-1}$	reaction rate constant
A_p	m^2	surface area of silica gel particles	K_{tot}	s^{-1}	overall transfer of h_2o from the particle to the gas bubbles
Ar	-	Archimedes number	k_{wall}	$Wm^{-1}K^{-1}$	tube wall thermal conductivity
B_{ads}	-	adsorption capacity of silica gel particles	k_{water}	$Wm^{-1}K^{-1}$	water thermal conductivity
C	-	normalized tracer concentration	L	m	initial height of particle column
$C_{p,water}$	$Jkg^{-1}K^{-1}$	heat capacity of water	m	kg	momentary mass of the oxygen carrier
$C_{H2O,b}^{in}$	kgm^{-3}	concentration of h_2o in the bubble phase entering the fb	$\dot{m}$	kgs^{-1}	rate of desorbed water
$C_{H2O,b}^{out}$	kgm^{-3}	outlet concentration of h_2o in the bubble phase exiting the fb	M_O	$kgmol^{-1}$	molar mass of oxygen
$C_{H2O,e}^{in}$	kgm^{-3}	concentration of h_2o in the emulsion phase entering the fb	m_{ox}	kg	mass of oxygen carrier in its fully oxidized form
$C_{H2O,e}^{out}$	kgm^{-3}	outlet concentration of h_2o in the emulsion phase exiting the fb	$m_{p,dry}$	kg	weight of dry silica gel particles
C_{H2O}^{in}	kgm^{-3}	inlet concentration of h_2o to the fb reactor	$m_{p,sat}$	kg	weight of saturated silica gel particles
C_{H2O}^{out}	kgm^{-3}	outlet concentration of h_2o from the fb reactor	$m_p(t)$	kg	weight of silica gel particles at each time during the desorption
$C_{H2O,b}^{ave}$	kgm^{-3}	average concentration of h_2o in the bubble phase	$n_i^{\cdot}$	$mols^{-1}$	molar flow rate of component i
$C_{H2O,e}^{ave}$	kgm^{-3}	average concentration of h_2o in the emulsion phase	$n^{\cdot}$	$mols^{-1}$	total molar flow rate at the reactor outlet
$C_{H2O,p}$	kgm^{-3}	concentration of h_2o in the particles	N	-	number of tanks in series
$C_{H2O,s}$	kgm^{-3}	concentration of h_2o on the surface of particles	p_{H2O}	Pa	partial pressure of H_2O
$C_{response}$	-	normalized detected tracer concentration leaving the reactor	Pr	-	Prandtl number
D	$m^2\ s^{-1}$	axial dispersion coefficient (paper VI, VII), molecular diffusion coefficient of gas (paper II, III)	Pe	-	Peclet number
D_c	m	column diameter	Q	W	heat transferred through tube wall
d_b	m	bubble diameter	Re	-	Reynolds number
d_P	m	average particle diameter	Sc	-	Schmidt number
d_i	m	inner tube diameter	Sh	-	Sherwood number
d_o	m	outer tube diameter	t	s	time
D/uL	-	vessel dispersion number	$t_{0.5}$	s	reaction's half-life
E	s^{-1}	exit age distribution	T_{bed}	K	bed temperature
F_o	Nm^3s^{-1}	volumetric fuel gas flow (20 °C, 1 atm)	$T_{wall,avg}$	K	average temperature of wall
F	-	fluidization number	$T_{wall,in}$	K	temperature of inside of tube wall
$F(X)$	-	integral form of $g(x)$	$T_{wall,out}$	K	temperature of outside of tube wall

Fs	kgs^{-1}	solid recirculation
g	ms^{-2}	gravitational acceleration
$g(X)$	-	extent of conversion
G_{air}	m^3s^{-1}	airflow to the fluidized bed
H	m	settled bed height
$H_{abs}^{in}(t)$	kgm^{-3}	inlet absolute humidity value at time t
$H_{abs}^{out}(t)$	kgm^{-3}	outlet absolute humidity at time t
h_i	$Wm^{-2}K^{-1}$	heat transfer coefficient from tube wall to water flow
h_o	$Wm^{-2}K^{-1}$	heat transfer coefficient from bed to tube
j_h	-	tube inside heat transfer factor
K_b	s^{-1}	transfer of h_2o from the emulsion to the bubble phase
K_{bc}	s^{-1}	interchange coefficient between bubble and cloud
K_{be}	s^{-1}	overall interchange coefficient between bubble and emulsion
K_{ce}	s^{-1}	interchange coefficient between cloud and emulsion
k_e	ms^{-1}	transfer of h_2o across the particles' surface and the emulsion gas
K_e	s^{-1}	transfer of h_2o across the particles' surface and the emulsion gas

$T_{water,avg}$	K	average water temperature inside tube
$T_{water,inlet}$	K	inlet water temperature
$T_{water,outlet}$	K	outlet water temperature
u, u_o	ms^{-1}	superficial gas velocity measured on an empty vessel basis
u_b	ms^{-1}	rise velocity of bubbles in fluidized bed
u_{br}	ms^{-1}	rise velocity of a single bubble with respect to the emulsion phase
K_{eq}	-	equilibrium constant
u_{mf}	ms^{-1}	minimum fluidization velocity
U_o	$Wm^{-2}K^{-1}$	overall heat transfer coefficient
u_{water}	ms^{-1}	water velocity inside tube
V	m^3s^{-1}	water flow rate
V_p	m^3	volume of silica gel particles
V_R	m^3	volume of reactor
X	-	oxygen carrier conversion
X	-	degree of water desorption from silica gel particles at each time
X_i	-	momentary conversion of component i
y_i	-	outlet volume fraction of gas component i

Greek letters

α	-	dimensionless number in reaction rate constant
δ	-	fraction of the bed in bubbles
Δm_{des}	kg	total quantity of desorbed water
ΔP_{bed}	Pa	pressure drop of bed
$\Delta P_{distributor}$	Pa	pressure drop over distributor plate
ΔP_{top}	Pa	pressure drop over the top region of the bed
ΔT_{LM}	K	logarithmic mean temperature
ΔT_{in}	K	inlet side temperature difference
ΔT_{out}	K	outlet side temperature difference
ε_{bed}	-	void fraction of fluidized bed
ε_e	-	voidage of the emulsion
ε_f	-	average void fraction in the fluidized bed

μ	Pas	gas viscosity
ρ_b	kgm^{-3}	bulk density of particles
ρ_g	kgm^{-3}	gas density
ρ_p	kgm^{-3}	particle density
ρ_{water}	kgm^{-3}	density of water
γ	-	fuel gas conversion
η	-	contact efficiency
ω	-	degree of oxygen carrier reduction
σ	Pa	standard deviation of pressure fluctuations
σ^2	s^2	variance of tracer curve
$\sigma_\theta{}^2$	-	normalized variance of tracer curve
ϕ_s	-	sphericity of particles

ε_{mf}	-	void fraction in the bed at minimum fluidization velocity	$\tau_0 = 0$	*s*	beginning of each experiment at which the tracer is injected into the FB
ε_p	-	fixed bed void fraction of bed particles	τ_1	*s*	time lag until the detection of the tracer at the outlet coil.
$\varepsilon_{p,packing}$	-	packing volume void fraction	τ	*s*	mean residence time of tracer in the FB

List of abbreviations

AR	air reactor	H_2	hydrogen
ASB	aluminum silicate balls	I.D.	inner diameter
BFB	bubbling fluidized bed	MEA	monoethanolamine
CCS	carbon capture and storage	N_2	nitrogen
CH_4	methane	PFR	plug flow reactor
CLC	chemical looping combustion	FCC	fluid catalytic cracking
CLG	chemical looping gasification	TGA	thermogravimetric analyzer
CO	carbon monoxide	TSA	temperature swing adsorption
CO_2	carbon dioxide	POC	post-oxidation chamber
CSTR	stirred tank reactor	RR	raschig ring
ECA	expanded clay aggregate	RTD	residence time distribution
FR	fuel reactor	SMR	steam methane reforming
FB	fluidized bed	SIR	steam-iron reaction

Table of Content

1 Introduction 13
1.1. Chemical- Looping Combustion 13
1.2. Mixing patterns and flow dynamics in fluidized bed reactors 16
1.3. Research space 18
1.4. Aim of the work 20
1.5. Outline of the thesis 20

2 Background 21
2.1 Packed-fluidized bed 21
2.2 Literature review 22
2.3 Framework 29

3 Method 31
3.1 Experimental 31
3.1.1 Chemical looping combustion 31
3.1.2 Heat transfer 33
3.1.3 Mass transfer 34
3.1.4 Residence time distribution 35
3.2 Modeling 37
3.2.1 Gas interchange 37
3.2.2 Mass transfer coefficient 38
3.2.3 Dispersion and tank-in-series models 39

4 Results 41
4.1 Fluidization and mapping of pressure drop 41
4.2 Bed-to-tube heat-transfer 43
4.3 Chemical looping combustion in packed-fluidized bed 44
4.4 Gas interchange coefficient in packed-fluidized bed 46
4.5 Particle to gas mass-transfer 48
4.6 Mass-transfer coefficient in packed-fluidized bed 49
4.7 RTD of solids in packed-fluidized bed 50
4.7.1 Cross-current flow reactor 50
4.7.2 Counter-current flow reactor 51

5 Summary and outlook 53
5.1 Discussion 54
5.1.1 High-void packings 54
5.1.2 Low-void packings 55
5.1.3 Implications for new technologies 56
5.2 Conclusion 57
5.3 Recommendations for further research directions 58

Appendix A– Methane Conversion 59

Appendix B– Syngas Conversion 60

References 61

1 Introduction

1.1. Chemical- Looping Combustion

The United Nations Sustainable Development Goals are the blueprint to achieve a better and more sustainable future for all. They address global challenges, including those related to poverty, inequality, climate change, environmental degradation, peace, and justice. The 17 Goals are all interconnected, and in order to leave no one behind, it is important that all be achieved [1]. Goal 13 to restrict global warming to well below 2°C above pre-industrial levels, was agreed upon in Paris in 2015 [2]. To meet this target, rapid decarbonization of all energy sectors is needed, together with large-scale deployment of negative-emissions technologies [3]. Carbon capture and storage (CCS) is a set of technologies that could reduce CO_2 emissions from point sources such as fossil power plants and industrial facilities. CCS involves securely storing captured carbon to prevent its release into the atmosphere, for example by injecting it into underground aquifers or depleted oil and gas wells. Depending on the carbon source, CCS can reduce the emissions of CO_2 from human activities to almost zero and may even result in net negative emissions. Negative emissions occur when CO_2 is directly or indirectly removed from the air and permanently stored in the process. An indirect method for achieving negative emissions is capturing the CO_2 generated from the combustion of biofuels for power and/or heat generation (Figure 1).

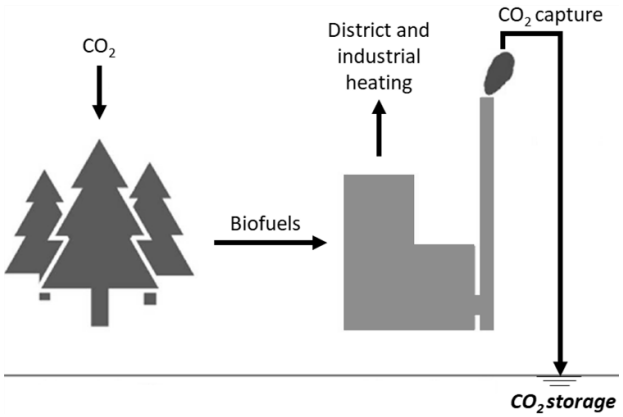

Figure 1. Illustration of the carbon flow in Bioenergy with carbon capture and storage.

The feasibility of different CO_2 separation methods from different processes has been acknowledged for many years. Therefore, many CCS projects employing technologies such as amine scrubbing, and oxy-fuel combustion have been initiated globally in the past decades [4]. Each evaluated technology exhibits distinct strengths and weaknesses in terms of cost, efficiency, and applicability [5]. Among the diverse CCS technologies, chemical looping combustion (CLC) is noted for its potential to capture CO_2 at relatively low costs both in terms of capital and energy, while also achieving a high capture rate [6–10]. In a conventional combustion system, fuel combustion occurs through its reaction with oxygen in air, resulting in a flue gas primarily consisting of nitrogen, mixed with excess oxygen and the main combustion products H_2O and CO_2. The high content of nitrogen results in relatively low CO_2 partial pressure in the flue gas, which complicates and increases the cost of CO_2 separation. CLC mitigates this issue by oxidizing the fuel with oxygen from solid metal oxide oxygen carriers instead of air [6]. The fundamental principle of CLC involves the use of two separate but interconnected reactors, typically referred to as the air reactor (AR) and the fuel reactor (FR). A simplified schematic of CLC is illustrated in Figure 2.

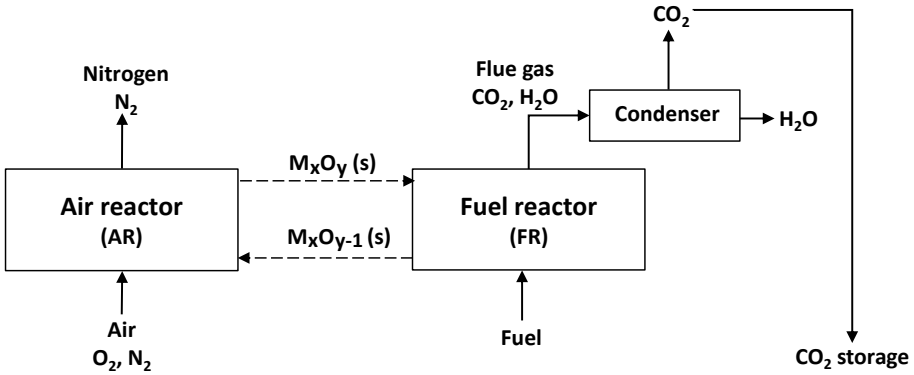

Figure 2. Schematic description of an idealized Chemical-Looping Combustion (CLC) plant.

As depicted in Figure 2, a solid metal oxide commonly referred to as the oxygen carrier (M_xO_y) facilitates oxygen transport between the two reactors. In the FR, the oxygen carrier reacts with and oxidizes the fuel (C_nH_{2m}). For solid fuels like biomass, this reaction is typically approximately adiabatic, but will depends on the specific fuel and oxygen carrier used [11]. The resulting products are a reduced oxygen carrier (M_xO_{y-1}), along with CO_2 and H_2O as flue gases. CO_2 capture in this system is more straightforward compared to conventional combustion processes, as the flue gas is not diluted with air. Thus, in the idealized case, H_2O can be separated from CO_2 via condensation, eliminating the need for complex gas separation systems. Subsequently, the reduced oxygen carrier is transported to the AR, where it undergoes re-oxidized to M_xO_y. This reaction is always exothermic, meaning that the AR and subsequent AR convection section is where heat will need to be extracted from the process. The general reduction-oxidation reactions for a gaseous or liquid fuel in the FR and AR reactors are represented by reactions (1) and (2).

$$C_nH_{2m} + (2n + m)M_xO_y \rightarrow nCO_2 + mH_2O + (2n + m)M_xO_{y-1} \quad (1)$$

$$M_xO_{y-1} + 0.5O_2 \rightarrow M_xO_y \quad (2)$$

In addition to gaseous and liquid fuels, solid fuels such as biomass are also extensively investigated in CLC, due to their abundance and high accessibility [12,13]. For the case of solid fuel, in the FR, the solid fuel undergoes decomposition into volatiles and char (C_nH_m) through

reaction (3), while the char is gasified to CO and H_2 via endothermic reactions (4) and (5). The oxidized form of the oxygen carrier (M_xO_y) supplies oxygen for the combustion of volatiles and gasification products in reaction (6). Direct solid-solid interaction between oxygen carrier and char is not expected to occur in a fluidized bed (FB) reactor. Following this, the reduced form of the oxygen carrier is then converted in the AR back to its initial state via a reaction similar to (2).

$$Solid\ fuel \rightarrow C_nH_m + Volatiles \quad (3)$$

$$C_nH_m + nH_2O \rightarrow nCO + (n + \frac{m}{2})H_2 \quad (4)$$

$$C_nH_m + nCO_2 \rightarrow 2nCO + (\frac{m}{2})H_2 \quad (5)$$

$$Volatiles, CO, H_2 + M_xO_y \rightarrow CO_2 + H_2O + M_xO_{y-1} \quad (6)$$

The CLC process generates two distinct outlet gas streams: oxygen-depleted air from the air reactor, and a mixture of CO_2 and H_2O from the fuel reactor. In an ideal case, pure CO_2 can be obtained by cooling the outlet flow from the fuel reactor and condensing steam into liquid water.

Conventional CO_2 capture methods by gas separation include techniques such as, oxy-fuel combustion, pre-combustion CO_2 capture, and post-combustion treatments [5]. Among these technologies, post-combustion CO_2 capture by monoethanolamine (MEA) scrubbing or analogous alkanolamine-based solvents have been a dominating solution for capturing CO_2 from combustion-derived flue gases. Nevertheless, this gas separation process involves high energy penalty, estimated to the order of a 10%-points reduction in power plant efficiency for large solid fuel plants, leading to a substantial increase, of approximately 30% or more, in fuel consumption and plant size [14]. This stands in sharp contrast to CLC, which in the idealized case does not suffer from energy penalty or increased plant size. Studies indicate that the cost of carbon capture in a large CLC solid fuel plant could be as low as 20 € per ton of CO_2 [15].

In addition to combustion, there are today also a number of chemical-looping technologies for syngas and hydrogen production, e.g. chemical-looping gasification (CLG) and reforming [16,17]. Most often in chemical-looping, fluidized-bed reactors are utilized. In such reactors, it is important to achieve high and uniform gas-solid mass and heat transfer, as this will enhance gas conversion. Fluidization was established as an industrially important concept in the 1940s, during which large-scale implementation of fluid catalytic cracking was introduced. The advantages of FB reactors include good heat and mass transfer rates, excellent gas-solid contacting, and temperature uniformity [18]. It soon extended its range of applications to other areas such as heat transfer, coating, drying, combustion, gasification, chemical reactors, and adsorption [19–21].

In the context of gas-solids fluidization, when a gas is introduced at low velocity in an upward direction through a bed of fine particles, it passes through the voids among the immobile particles, constituting what is referred to as a fixed bed. By increasing the flow rate, a point is reached where the particles are suspended by the fluid. The superficial gas velocity at this point is referred to as minimum fluidization velocity. At this velocity, the friction force between particle and fluid is equal to the weight of the particles, and the vertical component of the compressive force between adjacent particles disappears. Thus, the pressure drop throughout the bed equals the weight of fluid and particles inside the bed. Further increase in the fluid velocity beyond minimum fluidization results in the formation of gas bubbles and sometimes with channeling occurring inside the bed.

This is referred to as a bubbling-fluidized bed (BFB). For deep beds in narrow columns, the bubbles' diameter can become as large as the cross-section of the vessel. This mode of operation is called slugging and should preferably be avoided in practical applications. At even higher gas velocities, the terminal velocity of solids is exceeded, meaning that particles will be transferred upwards by the fluid flow. Depending on process conditions, turbulent fluidization or pneumatic transport of solids will ensue [18] (Figure 3).

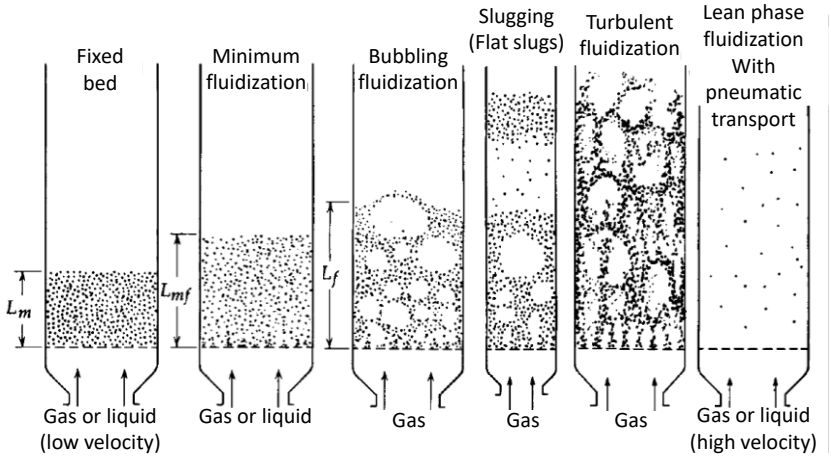

Figure 3. Illustration of fluidization regimes, by increasing the fluid velocity from left to right [18].

1.2. Mixing patterns and flow dynamics in fluidized bed reactors

As mentioned in the previous section, a BFB reactor is realized by passing a fluid stream, typically gas or vapor, upward through a bed of small solid particles at a flow rate sufficient to suspend the particles, causing thorough mixing of the solids. In this type of fluidized bed, the solid particles remain suspended without any net upward or downward flow, analogous to a continuous stirred tank reactor (CSTR) (Figure 4a). A CSTR maintains a state of thorough stirring and homogeneous concentration, ensuring that the composition of the exit fluid stream from the reactor mirrors that of the fluid within it [22,23]. A fluidized bed can have a fixed amount of particles or a throughflow of solids. For example, if solids are added at the top and removed from the bottom of the fluidized bed, there would be a downward flow of solid particles counter-current to the upward-flowing fluid. In both types of fluidized beds, it is generally desirable to reduce channeling of the fluid through the solid particles and the formation of stagnant zones of fluid or solid particles within the bed.

In the case of continuous flow of solid particles, it may also be desirable to minimize back-mixing of the solid particles and fluid within the fluidized bed, due to the detrimental effects back-mixing can have on the efficiency of the process. This second type of fluidization is analogous to a plug flow reactor (PFR) (Figure 4b). The defining characteristic of a PFR is the orderly flow of fluid through the reactor, devoid of any overtaking or mixing between consecutive elements in the direction of flow. While lateral mixing may occur within a PFR, no mixing or diffusion occurs along the flow direction, ensuring uniform residence time for all fluid elements [22,23].

Understanding the flow patterns of solids and gases in reactors with continuous solid flow is crucial for the performance of many fluidized bed applications. A fluidized bed exhibiting counter-current flow of fluid streams and solid particles is exemplified in applications such as strippers

and regenerators within fluid catalytic cracking (FCC) systems [24,25], as well as in temperature swing adsorption (TSA) processes, for instance, the adsorption of dilute carbon dioxide from flue gas streams [26–28].

In FCC systems, intermediate and high-boiling point hydrocarbons are atomized and brought into contact at high temperature with fluidized catalyst particles at high temperatures in a reactor. This interaction facilitates the cracking of hydrocarbons. Subsequently, the reaction products and catalyst particles are separated, typically using a cyclone. The catalyst particles are continuously removed from the reactor and undergo subsequent processing to maintain their effectiveness. Initially, they enter a catalyst stripper, where volatile hydrocarbons are removed from the catalyst in a fluidized bed by counter-currently contacting the catalyst with a flowing gas stream, such as water vapor (Figure 4c). The stripped catalyst particles are then directed to a regenerator, where the coke deposits and any residual hydrocarbons are removed by passing the catalyst particles through a fluidized bed counter-current to an oxidation gas, typically air.

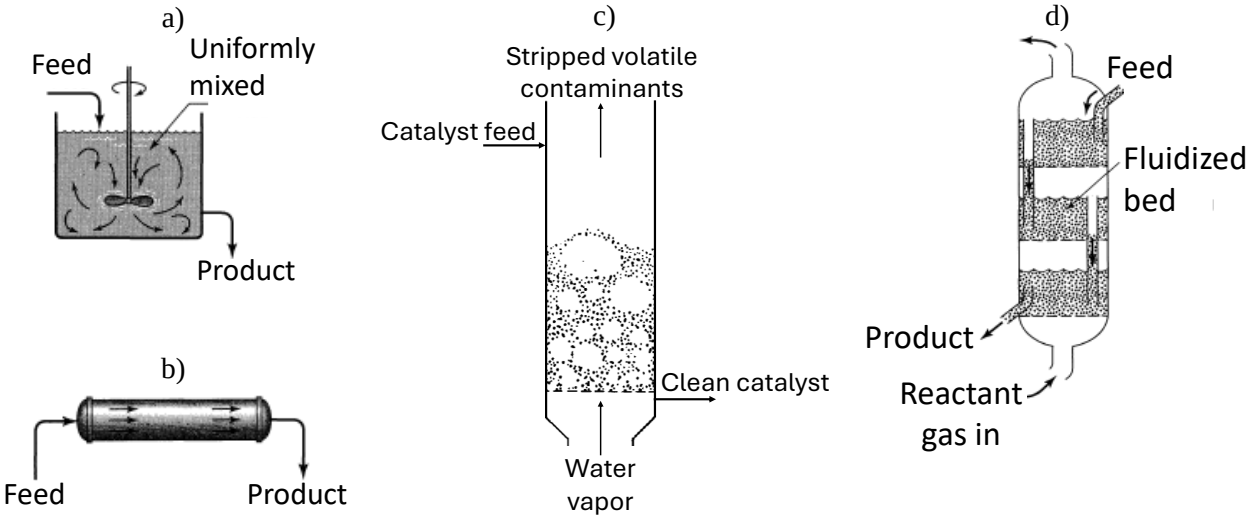

Figure 4. A schematic diagram of: a) CSTR, b) PFR, c) stripping process, d) staged reactor

Removal of these residual hydrocarbons from the catalyst in stripper is desirable because the hydrocarbons may be recovered and returned to the process as a reaction product, rather than being conveyed with the catalysts to the regenerator where they would be combusted, thereby causing an increase in air demand to the regenerator. Combustion of the residual hydrocarbons in the regenerator may also contribute to the degradation of the catalyst by subjecting the catalyst to elevated temperatures. In these fluidized beds found in the FCC stripper and regenerator, it would be desirable for all of the catalyst particles and the fluid streams to pass through the fluidized beds in a fully countercurrent fashion without channeling and back-mixing and with all catalyst particles and gas streams passing through the fluidized beds within defined time intervals, a condition known as plug flow, so that better and more predictable process efficiencies can be obtained [24].

Pröll et al. [26] introduced a trayed multi-stage two-circuit fluidized bed system for a continuously operated TSA process. This TSA process featured two columns: an adsorber and a desorber, each equipped with trays to facilitate the counter-current flow of solids and gas. In the adsorber column,

carbon dioxide from flue gas was adsorbed by the adsorbent in a gas-solid counterflow configuration. Solids moved downward from the uppermost fluidized bed to the lowermost bed via downcomers, while the gas flowed upward through the fluidized beds. The carbon dioxide-rich sorbent was then transported via a riser to the uppermost stage of the desorber column, where carbon dioxide was stripped by steam in a countercurrent motion and exited the column with the steam. The lean sorbent from the desorber's lowermost stage was cycled back to the adsorber (Figure 5).

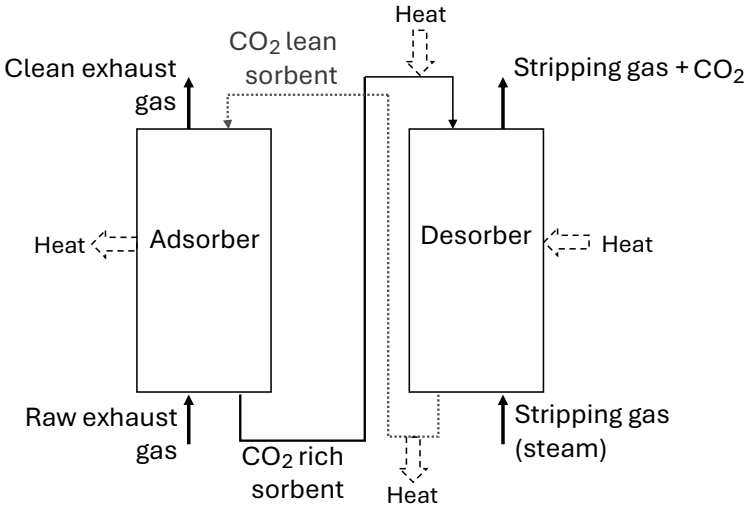

Figure 5. Schematic of the continuous temperature swing adsorption process [26].

Each stage in both columns was a BFB equipped with heat exchangers to manage the thermal requirements of adsorption and desorption. The scale-up efforts included modeling and simulation to optimize the number of stages in the adsorber and desorber, focusing on energy efficiency. For a separation task targeting a 90% carbon dioxide capture rate from a flue gas stream containing 10% carbon dioxide by volume, a configuration with five stages in each column was found to balance effort and efficiency effectively [26–28]. Concurrently, a bench-scale unit was used to validate the continuous operation of the proposed TSA process. However, parameter variation studies revealed that adsorber performance could be limited by solids flow patterns on the stages [28].

1.3. Research space

One challenging issue with FB reactors is the potential for reduced gas-solid mass and heat transfer at higher superficial gas velocities, especially when deep beds are used. This could occur due to bubble growth. It is easily realized that large bubbles result in reduced contact between gases and solids, and that ensuring good contact is necessary to achieve high gas-solid mass transfer and high heat transfer. Bubble growth could also lead to other undesirable fluidization phenomena such as slugging.

Another general challenge with FB reactors is the unoptimized flow patterns of solids and gases, leading to dead zones, channeling, particle back mixing, etc. In BFBs, certain reactions are equilibrium-driven [29,30], where the solid phase concentration rapidly reaches equilibrium. Thus, a counter-current or plug flow of the two phases can be advantageous to create a progressive

decrease in reactant concentration along the reactor's length and to enhance efficiency in such systems. However, large bubble formation and solid back mixing disrupt the plug flow behavior.

These factors are critical to technologies such as e.g. chemical-looping combustion (CLC). For example, in the context of CLC, undesirable phenomena such as bubble growth, slugging, or channeling, may result in a variety of issues including incomplete gas conversion, char loss to the air reactor, and the presence of elutriated char in the flue gas [15]. In practice, bubble growth in the CLC fuel reactor is expected to lead to insufficient contact of oxygen carrier particles and fuel, reduced fuel conversion, and reduced CO_2 sequestration [10,12,31]. Counter-current flow pattern would also increase the driving force for fuel conversion.

CLC pilot-scale operations have revealed that achieving complete gas conversion at reasonable costs presents significant challenges. Therefore, it is expected that an optimized full-scale CLC reactor may not achieve full combustion within the FR [15]. This would be unacceptable for good system performance and fulfilling requirements for CO_2 transport and storage [10]. Thus, the effluent flue gas from the FR necessitates further conversion through methods ensuring near-complete combustion, close to 100%, to get a pure CO_2 stream for storage purposes.

Consequently, the presence of unconverted fuel within the FR necessitates an additional procedure downstream of the FR cyclone to facilitate further combustion of fuel gases, volatiles, and char particles originating from the reactions in FR. The most commonly proposed procedure is the oxy-polishing step, which would be conducted in a post-oxidation chamber (POC). In the POC, pure oxygen serves as the oxidizing agent to achieve thorough combustion of the fuel components (see Figure 6). The residual fuel components typically correspond to an oxygen demand ranging from 5-30% [31], where a higher demand entails a greater energy penalty for oxygen production.

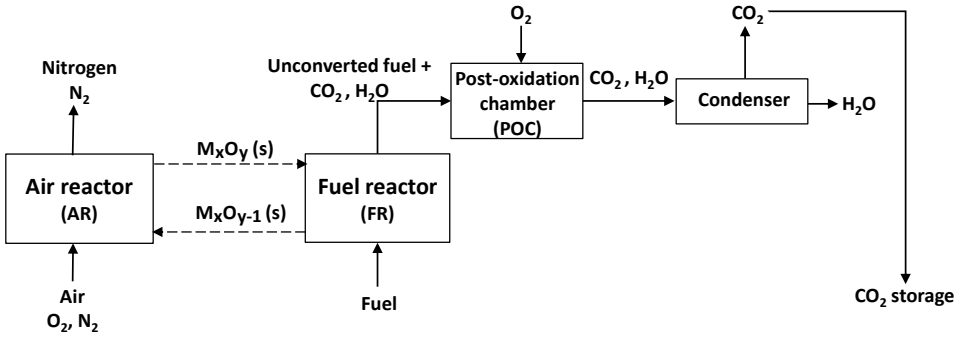

Figure 6. Schematic diagram of CLC with post-oxidation chamber (POC).

This challenge, therefore, lies in modifying the solid flow behavior inside the BFB reactor. Investigations into these issues have been limited [32]. Some researchers have proposed applying immersed baffles or tube bundles or changing the number of stages in the BFBs to break down large bubbles to smaller ones, prevent back mixing or to manipulate the RTD [33–35]. However, as mentioned, the incorporation of fixed parts to the FB such as e.g. tube bundles involve several challenges including erosion, complex maintenance, and potential obstacles with mechanical stress at elevated temperatures. Another alternative method proposed for operating fluidized beds in PFR mode is the utilization of moving bed reactors. For example, research conducted by Zhou et al. [36] , and Hsieh et al. [37] has recommended the implementation of moving beds in chemical

looping systems for hydrogen (H_2) production. Nonetheless, the use of moving bed reactors necessitates employing substantially large particles to prevent fluidization. It also requires very low fluidization velocities. Consequently, this leads to the necessity for reactors with significantly larger dimensions.

1.4. Aim of the work

The overall aim of this thesis is to introduce and examine a novel concept for BFBs that utilizes random packings, termed packed-fluidized bed or confined fluidization, and to contribute to the understanding of the role of the concept in mainly energy conversion processes. Such a broad aim can be analyzed with both experimental and modeling methods. Before the start of this thesis, there were very limited investigations conducted on packed-fluidized beds, and no detailed studies on heat and mass transfer and solids flow patterns. The thesis aims to bring together both perspectives of experimental and modeling methods to provide a comprehensive understanding of the challenges and opportunities of the concept. In pursuit of this goal, the study investigates the following specific aims:

- Fluidization behavior and mapping of pressure drop.
- Conversion of gaseous fuel in CLC reactions.
- Heat and mass transfer in bubbling fluidized beds.
- Gas interchange between bubble and emulsion.
- Residence time distribution of solids in the reactor.

1.5. Outline of the thesis

The thesis consists of a summarizing essay and seven appended papers. The summarizing essay consists of five thematic chapters that highlight the key outcomes of the papers and place the work in context. Following the introductory chapter, Chapter 2 introduces the packed-fluidized bed concept, and presents the scope of the seven papers. A short overview of the investigations on the packed-fluidized bed concept is also included in this Chapter. Chapter 3 provides the methodological details concerning the investigation on the packed-fluidized beds as outlined in the appended papers. This chapter is structured into two main sections experimental procedures and modeling approaches. In Chapter 4, the primary results are summarized. This includes:

- Investigation into pressure drop and segregation phenomena in packed-fluidized beds.
- Analysis of gas conversion behaviors in packed-fluidized beds within the context of chemical looping combustion (CLC) applications.
- Summary of results concerning mass and heat transfer in packed-fluidized beds, along with the outcomes of modeling efforts.
- Presentation of results on the residence time distribution (RTD) of solids in a packed fluidized bed, and the potential for achieving plug flow behavior through the application of packings.

Finally, Chapter 5 concludes the thesis with a summary of the overall results and suggestions for future research directions.

2 Background

This chapter provides an introduction to the packed-fluidized bed concept and a review of relevant literature exploring its previous applications.

2.1 Packed-fluidized bed

A conventional BFB can be divided into two main phases: the bubble phase or the diluted phase, which is mainly the fluidizing gas in the form of bubbles, and the emulsion phase or the dense phase, which contains both bed particles and gas (Figure 7). Previous studies showed that in a BFB, the mass transfer rate of gas between the bubble and emulsion phase decreases with an increase in bubble size [38,39]. While small bubbles are desirable for effective mass transfer, large bubbles can have the opposite effect by causing gas bypass and slugging [40]. One effective method to eliminate bubble growth in BFB is applying the concept of packed-fluidized beds [41–43]. In this method, inert stagnant packings of much larger size than the fluidized particles are applied to break down the larger bubbles, as illustrated in Figure 7b.

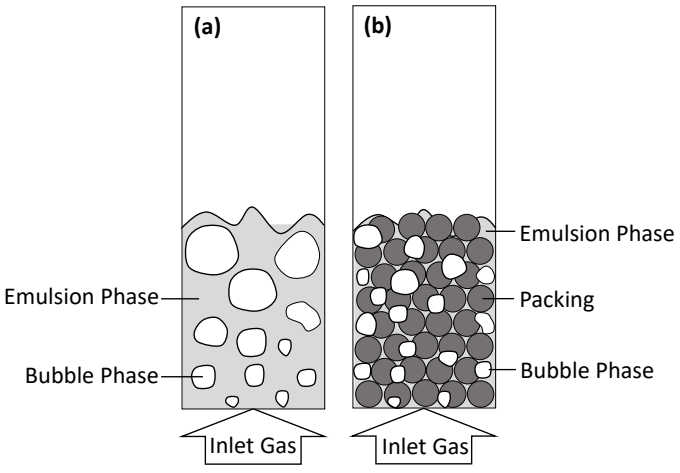

Figure 7. Illustration of a) conventional BFB, b) packed-fluidized bed.

The reactor can be filled with small objects like raschig rings, pall rings, saddle rings, etc. (random packing) or with a specifically designed structured packing (structured packing) (Figure 8).

a) b)

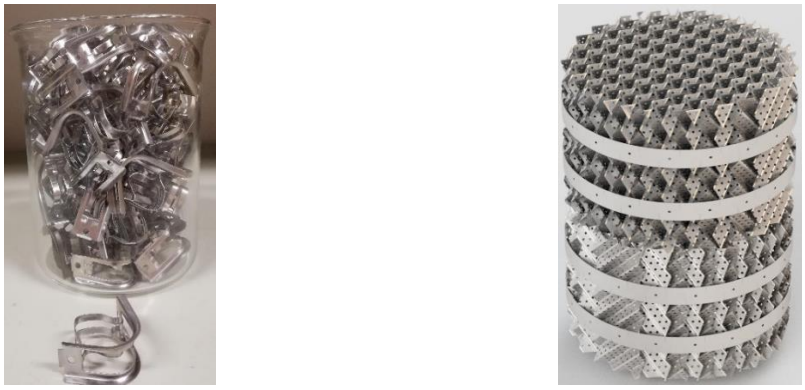

Figure 8. Packing types in packed beds: a) random packing, b) structured packing.

Random packings are very common to improve flow pattern, heat transfer and mass transfer in chemical reactor engineering. Packing material can be used instead of trays to improve performance e.g., in distillation columns. Packing offers the advantage of a lower pressure drop across the column (when compared to plates or trays), which is beneficial. Also, as mentioned above, other issues such as erosion and mechanical stresses can be avoided by applying random packings. Structured packing compared to random packing usually has a lower pressure drop but it is more expensive. Packing materials are characterized by factors such as specific surface area, void factor, and density. All of these parameters affect performance.

The void factor is a measure of the empty spaces in the packing. The void factor is a fraction of the volume of voids over the total volume, when packings are applied to a vessel. Using this definition, it will vary between 0 and 1. There are many ways to measure the void factor. For example, a straightforward experimental method can be applied as follows: i) An empty container is filled with water and weighed. ii) The container is then emptied and filled with packings. iii) Water is added to the packed container until it is completely full. iv) Then the container with packings and water is weighed. v) Dividing the weight of the water in the packed container by the weight of the water in the unpacked container gives the void factor. A high void factor indicates much empty space between packings. Thus, the fluid can flow easily through the packed zone. In general, in a high void packing, flow capacity is increased, and pressure drop is decreased, as compared to packings with a low void factor. The bulk density, also referred to as apparent density, is defined as the ratio of mass to the total volume. The bulk density of packings is measured by pouring them into a container with a known volume and similar diameter as the reactor vessel, while recording the changes in mass and dividing it by the volume of the container.

2.2 Literature review

Although packings have been used in a multitude of chemical reactor systems, the use of packings in fluidized beds has not been extensively studied. That said, few studies about the use of packed-fluidized beds have been presented in the literature, examining for example heat transfer [44–46], axial dispersion [47], bed expansion [48,49], and hydrodynamic behavior of gas-solid beds [50].

The effect of packings on fluidization was first investigated by Gabor and Mecham [51] and Sutherland et al. [41], who investigated the effect of spherical packings on hydrodynamics and heat transfer rates in FBs. They documented fundamental fluidization properties and observed that a combination of packed beds and FBs could improve the heat transfer rate. A few studies on packed-fluidized beds have been done afterward about topics such as catalytic reactions [52–55] and hydrodynamic properties such as minimum fluidization properties and pressure drop [43,50,56]. Donsi et al. [48] and Girimonte et al. [49] studied the expansion behavior of fine particles in a packed bed of spherical coarse particles at room temperature, in the velocity range up to 10 times the minimum fluidization velocity. Both research groups presented models for the bed expansion behavior of particles in a packed-fluidized bed, based on experimental results. The models describe hydrodynamic properties such as pressure drop, minimum fluidization velocity, and bed voidage. In another work, Girimonte et al. [57,58] investigated CO_2 adsorption on zeolite pellets in a packed-fluidized bed using glass spheres as packings. They observed that, for a given mass of sorbents, CO_2 adsorption increased compared to fixed beds, because of suppression of bubbles growth.

Aronsson et al. [38] successfully applied spherical packings in CLC batch experiments and found improved fuel conversion rates compared to a conventional BFB. However, there are no studies on other forms of packings and their effect on fuel conversion in this field of research. Also, the use of spherical packings in a FB may break down bubbles, but it could also constitute a major hindrance to fluidization. It may also influence factors such as the heat transfer rate significantly compared to non-packed beds [41]. Studies of fluidized-packed beds with evolved packing materials with high void factor and the impact on factors such as mass and heat transfer and particle segregation are lacking. Table 1 summarizes the most important investigations that have been done prior to this work on the packed-fluidized bed concept.

Table 1. Summary of investigations on packed-fluidized bed concept.

Packing	**Bed material**	**Results**	**Author. Year**	**Ref.**
Fixed stainless-steel strips coated by silver catalyst	Glass beads (inert bed)	- Silver catalyst for oxidation of ethylene to ethylene-oxide was sprayed on stainless steel strips which were attached to a centrally located supporting structure. - This method was examined to avoid agglomeration problems yet obtaining an excellent heat transfer property. - Small-scale tests with this method, showed that excellent temperature control could be achieved without serious adverse effects on catalyst performance.	Echigoya et al. 1960	[52]
Uniform spheres	Glass beads	- The effect of fixed packing on the properties of a gas-fluidized bed, including minimum fluidization velocity, pressure drop, and bed expansion was studied experimentally. - Experiments indicated that both packing size and the ratio of particle to packing diameter were the main variables in correlating the results. - A preliminary study was also made for heat transfer rates, and the results indicated that with spherical packing, values of heat transfer coefficient were of the order of 70% of that in a conventional bed.	Sutherland et al. 1963	[41]
Spheres and cylindrical packing	Glass beads, Aluminum oxide, copper	- Radial gas mixing in the voids of fixed packings was investigated. - Results showed that values of gas eddy diffusivities in the fluidized-packed beds were nearly the same as values in beds with the same type of packing but without the fluidizing materials. - Due to nonuniform pressure gradients associated with fluidization in packings, large variances in the eddy diffusion coefficient was observed compared to non packed beds.	Gabor et al. 1964	[59]

Table 1 (continued). Summary of investigations on packed-fluidized bed concept.

Packing	Bed material	Results	Author. Year	Ref.
Fixed stainless-steel cylindrical strips	α-Alumina and Glass beads	- Silver catalyst was sprayed on vertically mounted cylindrical strips for the strongly exothermic reaction of ethylene oxidation where the FB acted as an effective heat transfer medium in removing heat from the catalyst to the wall of the reactor. - They minimized the stagnant regions by this method and provided a good heat transfer from the catalyst surface. - Close temperature control was achieved so long as good fluidization around the packing was maintained. - For glass beads, poor fluidization was observed when sticking developed thus causing a large axial temperature profile.	McIlhinney et al. 1964	[53]
Spherical and cylindrical packings	Copper and nickel	- The lateral mixing behavior of particles fluidized in the voids of a packed bed is analogous to eddy diffusion in a flowing gas stream. - A model was used to relate the solids diffusivities to the void structure of the packed bed. - A dimensional correlation for solids diffusivity in a spherically packed bed was empirically deduced. - The rate of solids mixing increased with bed height for no packing but was independent of height for fluidized-packed beds.	Gabor. 1964	[60]
Spherical packing	Copper and nickel	- A model was developed to relate average particle velocity to the fluidizing gas velocity - A correlation for lateral solids mixing in a packed-fluidized bed was presented from the average particle velocity and the diameter of the fixed packing.	Gabor. 1965	[61]
Steel spheres	Cu-Ni, alumina and glass	- Effective thermal conductivities for lateral heat transfer were measured in a fluidized-packed bed. - A general correlation was made for the fluidized-packed bed thermal diffusivities with the size of the spherical fixed packing and the minimum fluidization velocity.	Gabor et al. 1965	[62]
Cylindrical screen packing (Pall ring)	silica-alumina cracking catalyst	- Effect of packing on the catalytic isomerization of cyclopropane in fixed and FBs were studied. - The effects of various cylindrical screen packing, on final conversion were determined. - Overall conversions were higher in a FB with packing than in a normal FB but were less than in a fixed bed. - Rate data from the fixed bed closely followed first-order kinetics. When the same catalyst was tested in a normal FB, the rate was dependent on linear gas velocity and catalyst bed height. With packing present in the FB, this dependency was much less, but packing size and shape had some effect.	Ishii et al. 1965	[54]
Cylindrical UO_2 pellets	An inert material	- Fluorination of depleted uranium pellets were studied in this work in a packed- fluidized bed system. - In their proposed system, the uranium pellets would be the packing solids and the fluidizing solids would be used as heat transport medium. - They investigated and formulated expressions for some basic fluidization phenomena such as pressure drop, solids mixing and bed expansion. - It was found that the addition of fluidizing solids increased the heat transfer coefficient by a factor two at the reactor walls, and eight at the top of the packing.	Anastasia et al. 1965	[63]

Table 1 (continued). Summary of investigations on packed-fluidized bed concept.

Packing	Bed material	Results	Author. Year	Ref.
Screen cylinders	Sand, Alumina, glass bead, cracking catalyst, polystyrene	- It was shown that a unique relationship between the relative velocity and the bed voidage did not exist. Consequently, simple batch measurements were not sufficient to describe the hydrodynamics of co- or counter-current flows (in contrast to liquid-solid fluidized systems. - A reason for the non-existence of this relationship was attributed to the fact that friction forces between packing and particles greatly contribute to the balance of forces for counter-current and also for batch systems.	Claus et al. 1976	[50]
Pall rings, Raschig rings and cylindrical screens	Silica-alumina catalyst (Geldart A)	- The hydrodynamic behavior of packed-fluidized beds regarding the gas-solid counter-current operation was investigated. - Pressure drop, hold-up, loading and flooding were evaluated and compared with literature data for gas-liquid systems. - They derived a correlation for the pressure drop, which was mainly caused by suspended particles.	Roes et al. 1979	[64]
Pall rings	Silica-alumina catalyst (Geldart A)	- The height of an overall mass transfer unit was measured in a gas-solid packed bed by steady state adsorption. -Then the mass transfer and axial dispersion was investigated for adsorption process with an extended model. - They showed that the height of true transfer unit was approximately independent of the solid mass flux and increased with increasing gas velocity. At low gas velocities axial dispersion of the gas and especially of the solid phase was the determining factor for column performance. At higher gas velocities mass transfer limitations became important.	Roes et al. 1979	[65]
Fixed packing of nickel on alumina catalyst	Alumina and glass beads	- kinetics and mass transfer for catalytic hydrogenation of ethylene in a packed-fluidized bed was investigated. - The mass transfer coefficient and reaction rate constant were evaluated from integral conversion data. - The mass transfer coefficient between the interstitially FB and the catalyst surface was correlated in dimensionless form.	Farrell et al. 1979	[55]
Tubes of square cross-section	Sand	- The heat transfer behavior of a counter-current gas-solid trickle flow contactor was studied. - Experimental data on the overall heat-transfer rate constant between the gas flow and the solid particle flow were obtained experimentally. - Pressure drop over the packings was low, while counter-current heat-transfer properties were remarkable. - Heat transfer behavior was described by a model based on single-particle flow and by incorporating the effect of particle agglomeration at higher solids fluxes.	Verver et al. 1986	[44]
Ceramic and glass raschig ring and catalyst pellets	FCC	- The pressure gradient and the static and the dynamic hold-up were measured for a system consisting of FCC trickling over a packed bed with a gas streaming in a counter-current flow. - A correlation for the pressure gradient in the preloading region was derived based on the Ergun equation and considering the internal gas recirculation due to the solid's trickles. - A correlation was given which related the boundary between preloading and loading with the particle and gas properties and the solids flow rate.	Westerterp et al. 1987	[66]

Table 1 (continued). Summary of investigations on packed-fluidized bed concept.

Packing	Bed material	Results	Author. Year	Ref.
Coarse spheres	Glass beads, FCC, alumina, copper	- They studied the expansion behavior of FBs of fine particles confined within packings of coarse spheres. - Throughout the whole expansion range, they proposed a general relationship between voidage and gas flow velocities, represented by a two-parameter power law of the Richardson-Zaki.	Donsì et al. 1989	[48]
Coarse spheres	Glass ballotini	- A model based on extension of the Blake-Kozeny equation to binary solid systems was developed to describe confined fluidization of fine particles. - Pressure drop, minimum fluidization velocity and expansion characteristics were determined for the studied bed material.	Donsì et al. 1990	[67]
Spherical elements (porcelain balls)	Sand	- A theoretical analysis based on an extension of the Ergun equation to bi-dispersed granular system was suggested for the correlations determining the minimum fluidization velocity.	Ziółkowski et al. 1992	[68]
Perspex rods	FCC	- The effect of packings on hydrodynamics (pressure drop and solids hold-up) was investigated at ambient conditions, for the riser part of a circulating fluidized bed (CFB) unit. - They showed that the pressure gradient over the packed section increased linearly with increasing solids mass flux, but faster than linearly with increasing applied gas mass flux. - They presented a correlation to describe the dynamic solids volume fraction. - The results of gas-solids mass transfer measurements for CFB unit were investigated.	van der Ham et al. 1994	[69]
Intalox saddles, raschig ring	FCC	- The pressure gradient and powder hold-up in the packing were measured in a rectangular FB. - A mathematical analysis for the prediction of pressure drop, which was caused by the powder hold-up and the friction between gas and packing and between powders and packing, were proposed.	song et al. 1995	[40]
-	-	- A review of fluid dynamics studies of counter-current gas-solid contactors were presented. - The experimental and mathematical models in research findings about the basic fluid dynamics parameters: flowing solids holdup, pressure drop and flow pattern were gathered.	Nikačević et al. 2007	[70]
Raschig rings, ceramic beads, crushed stone and glass Beads	Sand, propant, alumina and glass	- Static holdup was investigated experimentally and theoretically in packed-fluidized bed contactors. - The experimental results showed a significant influence of the geometry of the packing elements on static holdup. The physical properties of the flowing solids also influenced static holdup. A moderate influence of solids flux and a minor influence of gas velocity were observed. - An empirical correlation for the prediction of static holdup was developed from theoretical and numerical analyses.	Nikačević et al. 2009	[71]
Coarse spheres	Geldart B particles	- The dependence of bed voidage on fluidization velocity and particle properties was investigated. - Their analysis leaded to new relationships for calculating the parameters of the Richardson-Zaki correlation. Thus, providing a quantitative interpretation of the expansion process of packed-fluidized beds.	Girimonte et al. 2011	[49]
Spherical lead shots and spherical glass bead	Glass ballotini	- They investigated the criteria for obtaining a homogeneous fluidization in packed-fluidized bed. The criteria regarded: the choice of the size of particles constituting the packed bed and the packing height necessary to accommodate the desired level of voidage; the minimum aspect ratio of the confined bed that guarantees the minimum fluidization velocity to be independent of the bed mass; and the packed bed height required to operate the particle system over a broad field of homogeneous expansion.	Girimonte et al. 2013	[72]

Table 1 (continued). Summary of investigations on packed-fluidized bed concept.

Packing	Bed material	Results	Author. Year	Ref.
-	-	- A counter-current FB reactor for the dehydrogenation of olefins was patented. - The process utilized a reactor that included a slower flow of catalyst through the reactor, with a counter current flow of gas (process stream) through the catalyst bed.	Davydov et al. 2015	[73]
Active carbon, glass balls (Ballotini), activated alumina, silica gel	Glass balls	- Confined fluidization of fines in fixed bed of coarse particles was investigated. - Relations allowing calculation of the Richardson-Zaki-type equation coefficients, including description of inter-particle void and gas pressure drop in such systems were determined.	Buczek et al. 2016	[56]
Coarse spheres	Geldart B particles	- They presented a model to predict the minimum fluidization velocity of beds of Geldart's group B particles confined in a packed-bed of coarse spheres.	Girimonte et al. 2016	[74]
Spherical packing	Zeolites	- CO_2 adsorption by a FB of pellets of 13X zeolite was investigated. - The experiments compared the performance of a confined and that of a conventional FB at ambient temperature and pressure. - They demonstrated that confined fluidization improved the efficiency of the adsorption process compared to the conventional technique.	Girimonte et al. 2017	[57]
Lithium titanate (Li_2TiO_3) pebble	Li_2TiO_3	- Results showed that the effective thermal conductivity of packed-fluidized bed increased close to the value of thermal conductivity of pure Li_2TiO_3 at an optimum fluidization velocity corresponding to 2–3 times minimum fluidization velocity depending on fluidized particle, size, its volume fraction and wall temperature.	Mandal et al. 2017	[46]
Coarse glass sphere	Zeolite	- They performed CO_2 adsorption across a packed-fluidized bed compared with traditional fixed bed adsorption. - The packed fluidized system allowed operation across a wide-range of gas velocities without a substantial increase in pressure drop. -Packed-fluidized bed prevented the formation of bubbles in favor of enhancing the bed expansion ability.	Girimonte et al. 2019	[58]
Spherical packings (ECA, ASB)	Ilmenite	- Chemical-looping combustion with ilmenite as oxygen carrier was studied in a packed-fluidized bed with spherical packings. Syngas and CO was used as fuel at 915 °C. Results showed that in packed-fluidized bed, the effective reaction rate constant increased by up to a factor of 2 for a given bed mass compared to conventional FBs. - Up to 4 times less oxygen carrier bed mass was needed to achieve the same gas conversion in a packed-fluidized bed, at a lower total pressure drop.	Aronsson et al. 2019	[38]
Spherical packings (ECA, ASB)	Silica gel and olivine sand	- Packed-fluidized bed concept was applied to investigate the effect of packings on gas-solid mas-transfer. For mass transfer experiments the fluidizing air was humidified and the water adsorption rate onto silica gel particles acting as fluidizing solids was measured. - It was found that mass transfer increased by a factor of 1.9–3.8 with packing solids as compared to a non-packed reference. - Maximum vertical cross-flow was found to be significantly higher with low density packing (ECA) that fluidized, than with stationary high-density packing (ASB).	Aronsson et al. 2019	[43]
Spherical Al_2O_3	CuO/ Al_2O_3	- batch CLC in packed fluidized bed was investigated. - The axial temperature profile was diffusion-like. - The reactor experienced non-uniform radial temperature distribution and channeling affected the wall temperature profile. - There was a non-uniform distribution of oxygen carrier in the radial direction.	Guo et al. 2014	[75]

Table 1 (continued). Summary of investigations on packed-fluidized bed concept.

Structured packing	Liquid-solid fluidized bed	- The structured packing was examined as internal in liquid-solid fluidized beds. - The structured packing allowed expansion of the liquid velocity operation range before elutriation, promoting the liquid-solid mixing. - A correlation to estimate the bed expansion in structured packing was developed.	Piovano et al. 2014	[76]
Structured packing	Geldart A	- 3D CFD simulation was performed to compare the gas-solids flow hydrodynamics and bubble behaviors in a BFB. - The distributions of solids holdup and velocity were more uniform in the bubbling fluidized bed with structured packing than that without. - The bubble diameter in the packed bubbling fluidized bed was less than half. - The degree of gas back-mixing was reduced slightly while the degree of solids back-mixing was reduced by around 50% in the structured packed bubbling fluidized bed.	Zhao et al. 2019	[77]
Vertical internals	Geldart B	- Vertical internals led to 60% reduction in bubble volume. - A correlation was developed for bubble size and bubble rise velocity. - A scale-up approach was tested for catalytic fluidized bed reactors of Geldart B with vertical internals such as heat exchanger tubes. - With vertical internals, bubbles radial movement was slightly inhibited and bubble coalescence occurred more in axial direction.	Maurer et al.2014-2016	[78–80]
Structured packing	-	- An invention to create a counter-current flow pattern with structured packings in gas-solid fluidized beds. - The design was aimed to reduce channeling of the gas through the solid particles and the formation of stagnant zones. - The design reduce recirculation or back mixing of the solid particles.	Rall. 2001, Senegas 1998	[24, 25]

Through these investigations, it is clear that substantial advantages can be realized by the use of packed-fluidized beds. Possible advantages that have been identified include avoiding agglomeration for some special applications, improving the heat transfer properties, better temperature control, reducing the stagnant regions and improving fluidization, increased overall conversions and efficiencies, and elimination of bubble growth. Most of the studies presented in Table **1** were performed many decades ago with a few recent papers related to chemical-looping aspects.

Packed-fluidized beds could be of high interest for CLC and other applications. The reason is not difficult to grasp. For example, in CLC, it is absolutely critical to achieve a high mass-transfer rate between gas and oxygen carrier throughout the whole bed. This is because gaseous fuel species must get in physical contact with the solid oxygen carrier, in order to be converted to products. In contrast to normal FB combustion, in CLC, it cannot be expected that residual combustible components can be converted in the freeboard. Aronsson et al. investigated the effect of using spherical aluminum silicate balls (ASB) and expanded clay aggregate (ECA) as packings during CLC batch experiments [38]. They observed that these packings can improve fuel conversion. However, they could also result in increased pressure drop inside the bed and particle segregation phenomena [38,43]. Thus, there is still a lack of investigation for other types of relevant packings like the effect of a more evolved RMSR and Hiflow packings, and the theory behind the enhanced mass transfer. Hence, with the development and proposal of many new energy conversion technologies that utilize fluidized beds, such as CLC, packed-fluidized beds could play an important role in solving some of the challenges with respect to gas and solid conversion. Also,

in many new concepts, such as the steam reforming processes [29,81], multiple and connected fluidized bed reactors are utilized with gas-solid reactions occurring in each unit. Here it may be essential to optimize the solids flow pattern in order to overcome reaction and thermodynamic limitations. This may be challenging in a well-mixed fluidized bed, but here our conjecture is that packed-fluidized beds could provide a way to adjust and optimize solids flow and to achieve more plug-flow behavior. Such aspects have been little explored previously, see Table **1**, and is one of the main research ideas underlining this work.

2.3 Framework

The thesis is based on the utilization of different types of random packings within the packed-fluidized bed for different applications. For this purpose, seven distinct types of random packings are investigated and compared within this thesis. The examined packings are:

- 25 mm stainless steel thread saddle ring RMSR 25-3 (RMSR)
- 25 mm stainless steel pall ring Hiflow 25-5 (Hiflow)
- 12 mm expanded clay aggregates (ECA)
- 12.7 mm aluminum silicate balls (ASB 12.7)
- 6.3 mm aluminum silicate balls (ASB 6.3)
- 10 mm ceramic raschig ring (RR10)
- 6 mm ceramic raschig ring (RR6)

The main difference between these packings is their structure, void factor, material, and bulk density. RMSR and Hiflow can be categorized as being high void packings (void factor > 0.95), as compared to the others (with void factor < 0.6). Figure 9 and Table 2 outline these packings and their main characteristics.

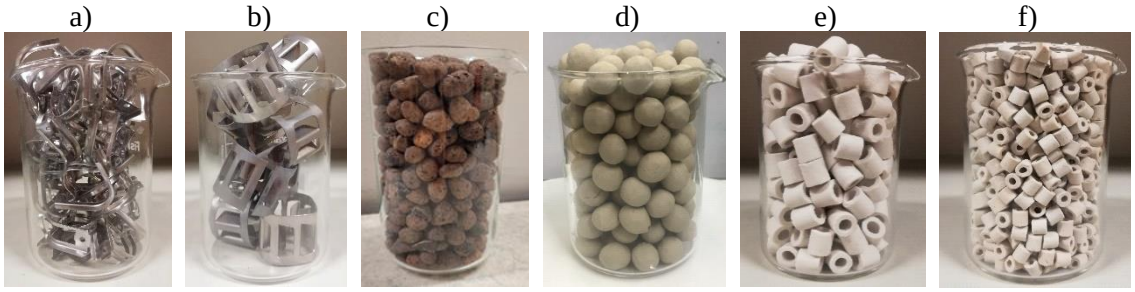

Figure 9. Packing materials investigated in this work: a) RMSR, b) Hiflow, c) ECA, d) ASB12.7, e) RR10, f) RR6.

Table 2. Experimental determination of the properties of packings.

Packing	**Void factor (-)**	**Bulk density (kg/m^3)**	**Paper**						
			I	**II**	**III**	**IV**	**V**	**VI**	**VII**
RMSR	0.96	204	■		■		■		
Hiflow	0.95	280	■		■		■		
ECA	0.58	280						■	■
ASB 12.7	0.43	1390	■	■		■			■
ASB 6.3	0.39	1468				■			
RR10	0.58	890	■						
RR6	0.50	1110							

In **Paper I**, the effect of five different types of random packings on heat transfer rate in a BFB is investigated. **Paper I** also investigate the effect of these packings on pressure drop and vertical segregation of fluidizing solids.

In **Papers II** and **III**, different selections of packings are considered from the above list and subjected to analysis in CLC batch experiments. **Paper II** compares two different fuels (CO and CH_4) in the beds containing RMSR and ASB packings. Then the results are benchmarked against bubbling beds without packings. In **Paper III**, the CO and syngas (50/50% H_2/CO) fuels conversions are compared for the beds containing the highly evolved packings of RMSR and Hiflow. Additionally, a model is introduced in **Paper III** to evaluate the impact of packings on the bubble size and gas interchange coefficient in the bed.

In Paper V, the impact of random packings on the gas-solids mass transfer in a BFB is studied. To achieve this aim, targeted experiments in a bed of moist silica gel are performed, in which the rate of H_2O desorption is monitored for free bubbling and fluidized-packed bed conditions. Detailed analysis of the mass transfer is done through a model accounting for the different steps in the mass transfer chain.

Paper IV investigates the influence of ASB packings on solid flux. Subsequently, **Papers VI** and **VII** explore the effects of utilizing random packings on residence time distribution and mixing characteristics within a BFB. **Paper VI** specifically analyses cross-current flow with continuous solids throughflow, while **Paper VII** focuses on counter-current flow with continuous solids throughflow. A summary of the appended papers and their contribution to this work is presented in Figure 10.

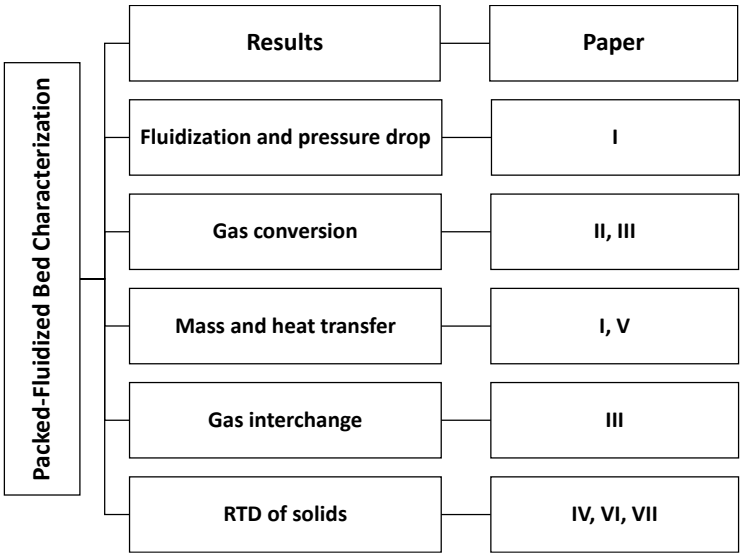

Figure 10. Summary of investigations on the concept of packed-fluidized bed.

3 Method

This chapter provides a summary for the experimental and modeling approaches discussed in the appended papers (**Papers I-VII**).

3.1 Experimental

3.1.1 Chemical looping combustion

Detailed information about the dimensions of the laboratory-scale BFB reactor utilized for the CLC experiments is summarized in Table 3.

Table 3. Summary of the two laboratory experimental setups used for CLC and heat transfer experiments.

Specification	**Papers I- III**
Reactors:	
I.D. (mm)	78
Height (mm)	1270
Distribution plates:	
Type	Circular hole plate
Thickness (mm)	5
Number of holes (-)	61
Hole I.D. (mm)	0.6

In **Papers II-III**, the impact of packed-fluidized bed on fuel conversion rate in CLC is investigated. A schematic description of the batch CLC reactor used in **Papers II-III** is shown in Figure 11. The composition of the outlet gas is measured with a gas analyzer SICK GMS810. Sampling is done via a PTFE tube heated to 190 °C, to ensure that condensation prior to the gas conditioning system does not occur. The SICK GMS810 gas analyzer measures the composition of dry gas in volume percent (vol%) for relevant gas components, including CO_2, CO, H_2, CH_4, and O_2.

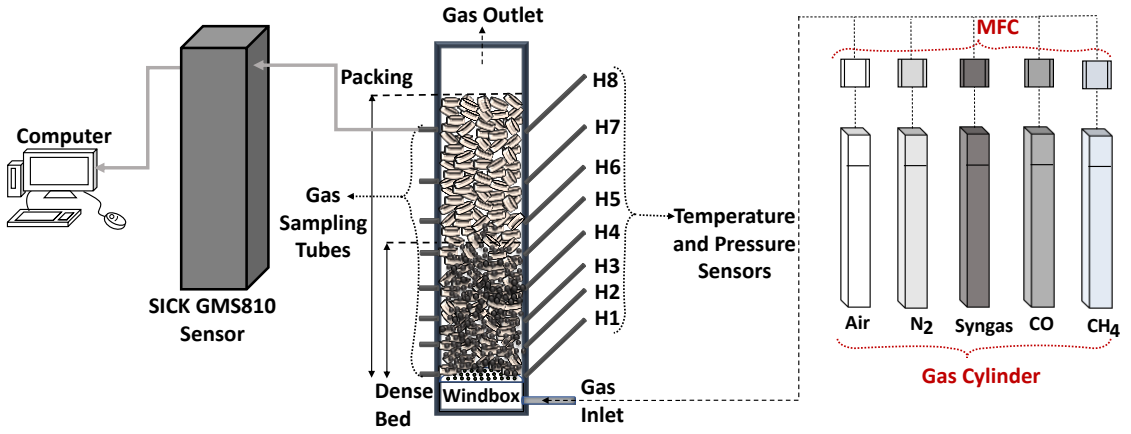

Figure 11. Schematic illustration of reactor for batch CLC reactions in Papers II-III.

In **Papers II–III** ilmenite concentrate is chosen as the bed particles and oxygen carrier. The reason is that this is the best studied and possibly the most reliably performing oxygen carrier for CLC. Ilmenite concentrate is the crushed and beneficiated form of the mineral ilmenite, which is an ore mined for the production of TiO_2. Ilmenite ore consists mainly of iron and titanium oxides ($FeTiO_3$, Fe_2TiO_5, Fe_2O_3, TiO_2, Fe_3O_4). Ilmenite concentrate is ilmenite ore that has been ground and physically beneficiated to increase the content of iron and titanium oxides. In **Papers II–III**, the ilmenite particles were originally generated in a CLC campaign by Moldenhauer et al. [82], and have previously been used in other experimental studies [38,83]. The reason for using this batch of material is to ensure that the particles had undergone hundreds of redox cycles and reached steady-state conditions, as fresh ilmenite used for CLC experiences swelling and activation during the first few dozens of redox cycles. The measured bulk density of the particles used is 1637 kgm^{-3}. The ilmenite particles are sieved to the size range 90-250 µm. The average diameter of particles is 179 µm.

In **Paper II**, investigated fuel gases are carbon monoxide (CO) at 840 °C and methane (CH_4) at 940 °C. The reason for using these fuel gases is the well-established difference in the reaction rate in CLC for these two gases when using ilmenite as oxygen carrier. Thus, since the aim of the study is to examine the impact of packing materials, rather than the impact of temperature on the reactivity of ilmenite with fuel gases, the temperature levels are chosen so that high but not complete fuel conversion can be expected. By doing so, any improvement when using packings could be seen clearly. In **Paper III**, fuel gases were syngas (50/50% H_2/CO) and CO at 840 °C. Syngas is a representative fuel for practical applications. CO is used since it simplifies data evaluation and can make it easier to draw firm conclusions and support modeling. In **Papers II-III**, nitrogen (N_2) is used as the inert gas. Air is used as oxidizing gas. For the gas fuels used in **Paper II** (CO and CH_4) and **Paper III** (CO and syngas, 50/50% H_2/CO) conversion equations are listed in Table 4. Additional details regarding the derivation of the momentary conversion of oxygen carrier are provided in the Appendix.

Table 4. The equations used to calculate fuel conversion in Papers II- III.

Fuel conversion:		
Conversion of CO (-)	$\gamma_{CO} = \frac{\dot{n}_{CO_2,out}}{\dot{n}_{CO,out} + \dot{n}_{CO_2,out}}$	(7)

Table 4 (continued). The equations used to calculate fuel conversion in Papers II-III.

Conversion of CH_4 (-)	$\gamma_{CH_4} = \frac{\dot{n}_{CO_2,out}}{\dot{n}_{CH_4,out} + \dot{n}_{CO_2,out} + \dot{n}_{CO,out}}$	(8)
Conversion of syngas (-)	$\gamma_{syngas} = \frac{\dot{n}_{CO_2,out} + \dot{n}_{H_2,in} - \dot{n}_{H_2,out}}{\dot{n}_{CO,out} + \dot{n}_{CO_2,out} + \dot{n}_{H_2,in}}$	(9)
Conversion of H_2 (-)	$\gamma_{H_2} = \frac{\dot{n}_{H_2,in} - \dot{n}_{H_2,out}}{\dot{n}_{H_2,in}}$	(10)
Conversion of oxygen carrier:		
Oxygen carrier conversion (-)	$X = 1 - \frac{m}{m_{ox}}$	(11)
Momentary conversion for CO (-)	$X_i = X_{i-1} + \int_{t-1}^{t} \frac{\dot{n} M_O}{m_{ox}} (y_{CO_2}) dt$	(12)
Momentary conversion for CH_4 (-)	$X_i = X_{i-1} + \int_{t-1}^{t} \frac{\dot{n} M_O}{m_{ox}} (4y_{CO_2} + 3y_{CO} - y_{H_2}) dt$	(13)
Momentary conversion for syngas (-)	$X_i = X_{i-1} + \int_{t-1}^{t} \frac{\dot{n} M_O}{m_{ox}} (2y_{CO_2} + y_{CO} - y_{H_2}) dt$	(14)

3.1.2 Heat transfer

The reactor employed in the heat transfer experiments shares the same furnace and much of the infrastructure with the CLC reactor. More detailed information about the common dimensions of the two laboratory-scale BFB reactors are summarized in Table 3. In **Paper I**, the effect of packed-fluidized bed on heat transfer at elevated temperature levels is studied. Figure 12 provides a schematic illustration of the reactor used in **Paper I**.

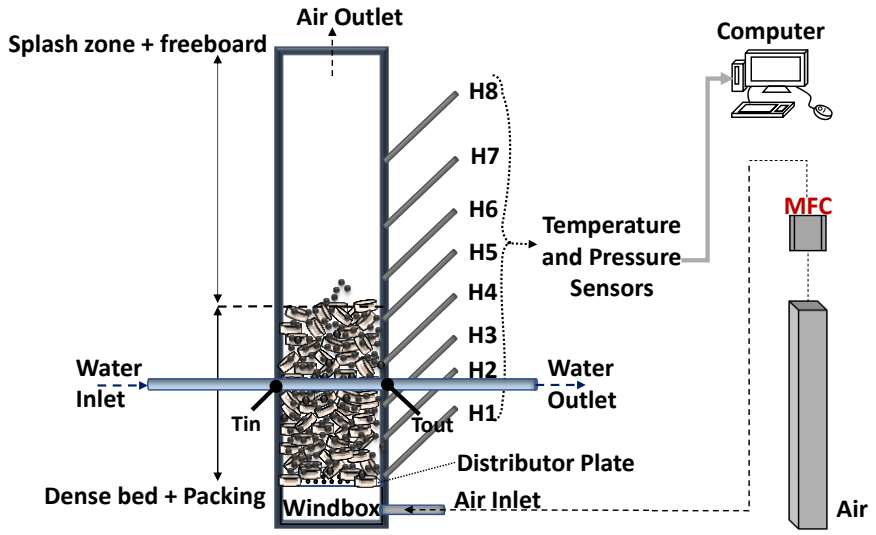

Figure 12. Schematic illustration of reactor for heat transfer experiments, used in Paper I.

For **Paper I**, a 253 MA steel reactor is equipped with a single horizontal tube made of Inconel 600 alloy. The inner diameter of the horizontal tube is 4 mm, and the wall thickness is 1 mm. The horizontal tube is positioned 75 mm above the gas distributor plate. In all experiments, the horizontal tube is in the dense bed; and it is covered with the packing and bed material. Water

flows through the horizontal tube from a tap. The flow rate is regulated with a valve. During all experiments, the water flow rate through the pipe used for measuring the heat transfer coefficient is kept constant at 20 mls^{-1}. In **Paper I**, the bed material used in experiments is silica sand supplied by Sibelco Nordic AB. It is sieved to the size range of 90-400 µm. The mean particle diameter is calculated to 240 µm. The bulk density of the bed material used in **Paper I** is 1594 kgm^{-3}. Air is used as the fluidizing gas for the experiments in **Paper I**. Superficial gas velocity is varied in the range of 0.04-0.411 ms^{-1}.

Bed-to-tube heat transfer coefficient, h_o, was calculated applying the overall heat transfer coefficient formula through a tube. The equations used to calculate h_o in **Paper I** are summarized in Table 5 [84–86].

Table 5. The equations used to calculate h_o in Paper I.

Bed-to-tube heat transfer coefficient	$h_o = \frac{1}{\frac{1}{U_o} - \frac{d_o \ln(d_o/d_i)}{2k_{wall}} - \frac{d_o}{d_i h_i}}$	(15)
Overall heat transfer coefficient (Wm^{-2}K^{-1})	$U_o = \frac{Q}{A_o \Delta T_{LM}}$	(16)
Logarithmic mean temperature (K)	$\Delta T_{LM} = \frac{\Delta T_{in} - \Delta T_{out}}{\ln(\Delta T_{in}/\Delta T_{out})}$	(17)
Inlet side temperature difference (K)	$\Delta T_{in} = T_{bed} - T_{water,inlet}$	(18)
Outlet side temperature difference (K)	$\Delta T_{out} = T_{bed} - T_{water,outlet}$	(19)
Heat transfer rate between bed and water flow	$Q = \rho_{water} \dot{V} c_{p,water} (T_{water,outlet} - T_{water,inlet})$	(20)
Heat transfer coefficient from tube wall to water (Wm^{-2}K^{-1})	$h_i = 0.023 \frac{k_{water}}{d_i} Re^{0.8} Pr^{0.4}$	(21)
	$h_i = \frac{k_{water}}{d_i} j_h Re Pr^{0.33}$	(22)
	$h_i = \frac{4200(1.35 + 0.02 T_{water,avg}) u_{water}^{0.8}}{d_i^{0.2}}$	(23)
Temperature of inside of tube wall (K)	$T_{wall,in} = \frac{Q}{h_i A_i} + T_{water,avg}$	(24)
Temperature of outside of tube wall (K)	$T_{wall,out} = Q \frac{d_o \ln(d_o/d_i)}{2k_{wall \times} A_o} + T_{wall,in}$	(25)

3.1.3 Mass transfer

In **Paper V**, a detailed experimental and modeling study is conducted with the aim of flushing out and explicitly determining the effect of packings on mass transfer in a fluidized bed. One motivation for this set of experiments is to conduct a more in-depth investigation of mass transfer phenomena, where kinetic effects are either eliminated or significantly simplified. Cold-flow reactors are used and silica gel particles are selected as bed material due to their high moisture adsorption capacity. The bulk density of the silica gel particles is measured to 680 kgm^{-3}, and the particles are sieved to the size range of 355-2100 µm, resulting in a Sauter particle diameter of 797 µm. The adsorption and desorption experiments are carried out in a transparent cylindrical acrylic column of 1.5 m in height and an inner diameter of 22 cm. The column is equipped with two humidity sensors to sample water content in the input and outlet gas. For experiments in **Paper V**, the system is filled with 4 kg of silica gel. Then, the fluidization number is set to F=1.7.

Subsequently, the inlet air temperature is set to 30°C employing a pre-heater, before its introduction into the humidifier. Owing to heat losses to the environment in the humidifier and the piping before the bed, the FB exhibits a slightly lower temperature. At steady state, the inlet air temperature is around 25°C. Figure 13 provides a schematic illustration of the reactor used in **Paper V**.

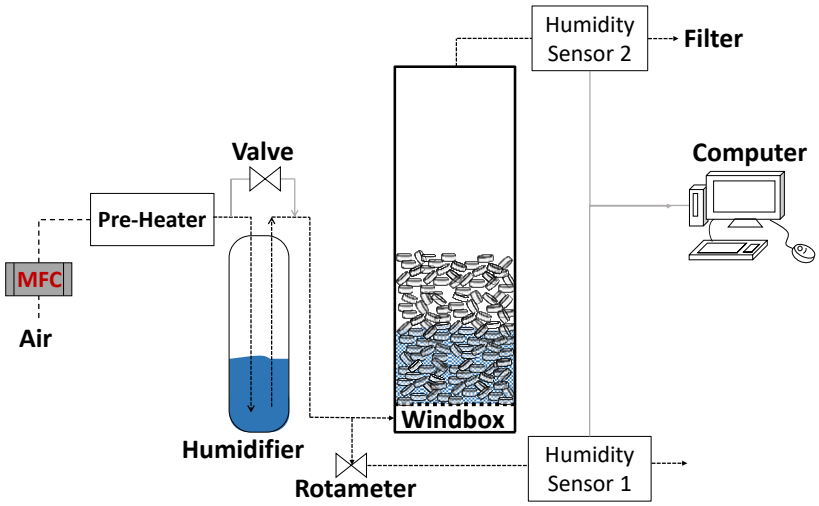

Figure 13. Schematic diagram of experimental setup for mass transfer experiments, used in Paper V.

In **Paper V**, a desorption analysis time of 2 h was found suitable for the data analysis, as longer time frames provided no additional information. The adsorption capacity and desorption kinetics of silica gel particles are determined by experiments in a thermogravimetric analyzer (TGA) with a sensitivity of 0.1 µg. The equations used to analyze the experimental data in **Paper V** are summarized in Table 6.

Table 6. The equations used to calculate the water desorption rate in Paper V.

Adsorption capacity of silica gel (-)	$B_{ads} = \frac{m_{p,sat} - m_{p,dry}}{m_{p,dry}}$	(26)
Instantaneous water desorption rate (kgs^{-1})	$\dot{m}(t) = G_{air}\left(H_{out}^{abs}(t) - H_{in}^{abs}(t)\right)$	(27)
Total quantity of water desorbed from silica gel particles (kg)	$\Delta m_{des} = \int_0^{t_f} \dot{m}(t)dt$	(28)

3.1.4 Residence time distribution

Papers VI-VII investigate the influence of employing random packings on the residence time distribution and mixing characteristics of solids in a BFB. To fulfill this objective, experiments are conducted using two different BFB cold-flow model reactor systems, providing counter-current flow, **Paper VII**, and cross-current flow, **Paper VI**, with continuous solids exchange. The two reactor systems have different sizes, shapes, and flow patterns, which is helpful to assess the effects of physical parameters on the experimental results and to make the results representative. The reactor used in **Paper VII** consists of a cylindrical Plexiglas acrylic reactor column with an inner diameter of 12 cm and a height of 1 m. A device is used to allow the pouring of fluidizing solids at a constant rate on top of the reactor. It consists of a funnel-shaped reservoir with sharply inclined walls, where the bottom opening is attached to a ball valve. At the bottom of the cylindrical column, a pipe with an internal diameter of 30 mm and length of 75 mm is aligned

with a 45° angle with respect to the reactor body. A ball valve is installed at the pipe's outlet to regulate the discharge rate of solid particles to match the inlet solid mass flow rate. As depicted in Figure 14, this setup allows for establishing a net counter-current flow of gas and solids.

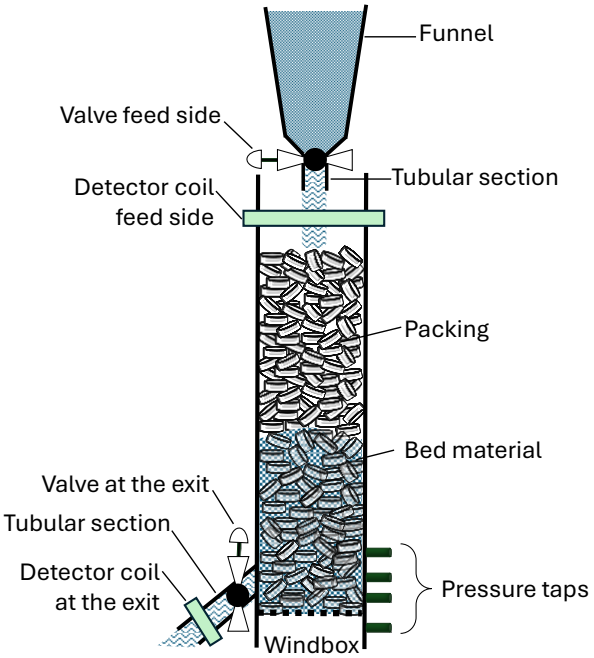

Figure 14. The cylindrical laboratory-scale cold flow model setup, used in Paper VII.

The setup for the cross-current flow experiments was previously designed and described by Hofer et al. and is illustrated in Figure 15 [32,34,87].

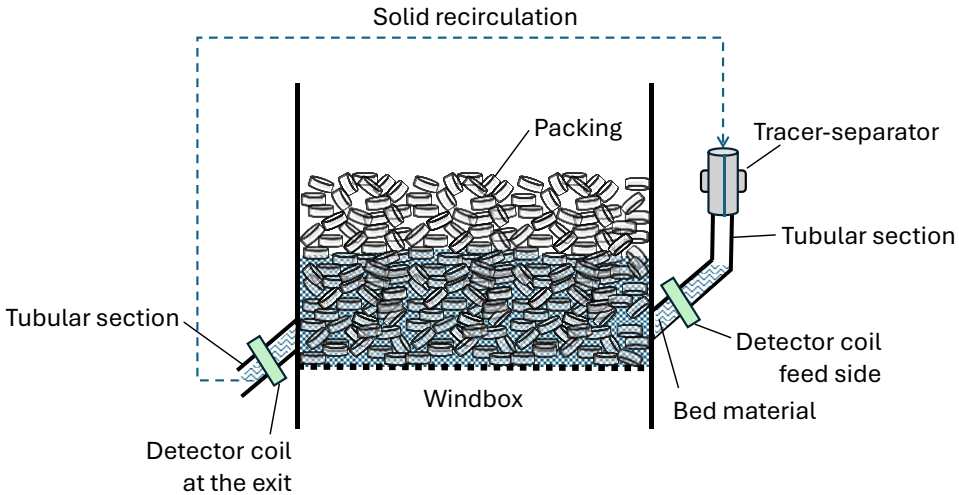

Figure 15. The rectangular cuboid laboratory-scale cold flow model setup, used in Paper VI.

The chamber of the FB has cross-sectional dimensions of 0.4 m in length and 0.2 m in width, with an overall height of the BFB reaching approximately 0.4 m. During operation, particles are continuously extracted from the FB, recirculated, and introduced opposite the point of withdrawal, creating a net cross-current flow of gas and solids. Further details about this configuration can be found in the works of Hofer et al. [32,87] and Eder et al. [34]. The properties of the used bed materials and tracers in **Papers VI-VII** are detailed in Table 7.

Table 7. Bed material and tracer properties in Papers VI-VII.

Reactor type		Counter-current flow		Cross-current flow	
Material		Inert	Tracer	Inert	Tracer
Properties	Unit	Olivine Sand	Magnetite	Glass bead	Stainless steel 1.4742
d_p	μm	120	90	130	72
ρ_p	kgm^{-3}	2700	5100	2450	7579
ρ_b	kgm^{-3}	1603	2626	1570	n/a
Ar	-	163	130	188	99
u_{mf}	ms^{-1}	0.016	0.017	0.017	0.016

The equations used to analyze a pulse input of the ferromagnetic tracer to the FB in **Papers VI-VII** are summarized in Table 8.

Table 8. The equations used to calculate the RTD in Papers VI-VII.

Area under the $C_{response}$-curve (s)	$A = \int_0^\infty C_{response,t}\,dt \cong \sum_t C_{response,t}\,\Delta t_i$	(29)
E-curve (s^{-1})	$E(t) = \frac{C_{response,t}}{A}$	(30)

3.2 Modeling

3.2.1 Gas interchange

In **Paper III**, the effective reaction contact factor, which is the multiplication of contact efficiency and reaction rate constant for the combustion experiments, is estimated as k_f ($Nm^3kg^{-1}s^{-1}$). Further, packings affect the reaction rate through changing the mass transfer rate between bubble phase and emulsion phase. This is believed to be one of the principal bottlenecks for converting fuel to CO_2 with CLC (**Papers II-III**). In other words, packings affect the mass transfer rate by changing the surface area between bubbles and emulsion, through affecting the bubble size. Thus, in **Paper III**, a model for calculating average bubble size, d_b (m), and then, the overall interchange coefficient between the bubble phase and emulsion phase, K_{be} (s^{-1}) is introduced (Figure 16).

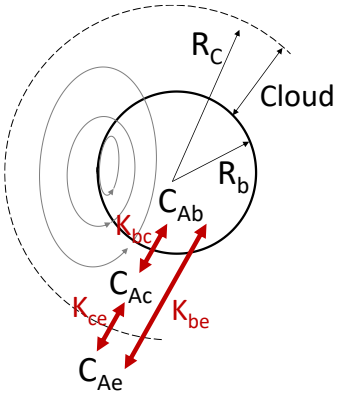

Figure 16. Gas streamlines and illustration of exchange coefficients near a single rising bubble in a clouded bubble, source: Paper III.

For this purpose, the two-phase theory model is applied in which emulsion stays at minimum fluidizing condition. Further details of the applied model are provided in Table 9.

Table 9. Reaction contact factor and gas interchange coefficient presented in Paper III.

Effective reaction contact factor ($Nm^3kg^{-1}s^{-1}$)	$k_f = \eta \times k_r = \frac{\alpha F_0}{m}$	(31)
Overall gas exchange coefficient between bubble and emulsion (s^{-1})	$K_{be} = \frac{1}{\frac{1}{K_{bc}} + \frac{1}{K_{ce}}}$	(32)
Gas exchange coefficient between bubble and cloud (s^{-1})	$K_{bc} = 4.5\left(\frac{u_{mf}}{d_b}\right) + 5.85(\frac{D^{1/2} g^{1/4}}{d_b^{5/4}})$	(33)
Gas exchange coefficient between cloud and emulsion (s^{-1})	$K_{ce} = 6.77\left(\frac{D\varepsilon_{mf} u_{br}}{d_b^3}\right)^{1/2}$	(34)
Minimum fluidization velocity (m s^{-1})	$\frac{d_p u_{mf} \rho_g}{\mu} = \left[(28.7)^2 + 0.0494\left(\frac{d_p^3 \rho_g (\rho_p - \rho_g) g}{\mu^2}\right)\right]^{1/2} - 28.7$	(35)
Void fraction in bed at minimum fluidization (-)	$\frac{1.75}{\varepsilon_{mf}^3 \emptyset_s}\left(\frac{\rho_P u_{mf} d_P}{\mu_g}\right)^2 + \frac{150(1-\varepsilon_{mf})}{\varepsilon_{mf}^3 \emptyset_s^2}\left(\frac{\rho_P u_{mf} d_P}{\mu_g}\right) = Ar$	(36)
Void fraction in the FB (-)	$\varepsilon_f = 1.5\left(\frac{\sigma}{0.438 \rho_P g L}\right)^{0.8896} Ar^{-0.0211}(\frac{L}{D_c})^{-0.388}$	(37)
Bubble diameter (m)	$d_b = \frac{1}{(0.711)^2 g}\left[u_{mf} + (u_o - u_{mf})\frac{1-\varepsilon_{mf}}{\varepsilon_f - \varepsilon_{mf}}\right]^2$	(38)

3.2.2 Mass transfer coefficient

In **Paper V**, a model for desorption in gas-fluidized beds is developed. In this model, the overall mass transfer coefficient, K_{tot}, is broken down into the three constitutive sequential steps, as illustrated in Figure 17: i) the transfer of water from internal particle sites to the particle surface (which entails both kinetics and intra-particle mass transfer and is characterized through the transfer coefficient K_p), ii) the mass transfer of gas across the boundary between the particle surface and the emulsion gas (characterized through the coefficient K_e), and iii) the mass transfer from the emulsion gas to the bubble phase (characterized through the coefficient K_b).

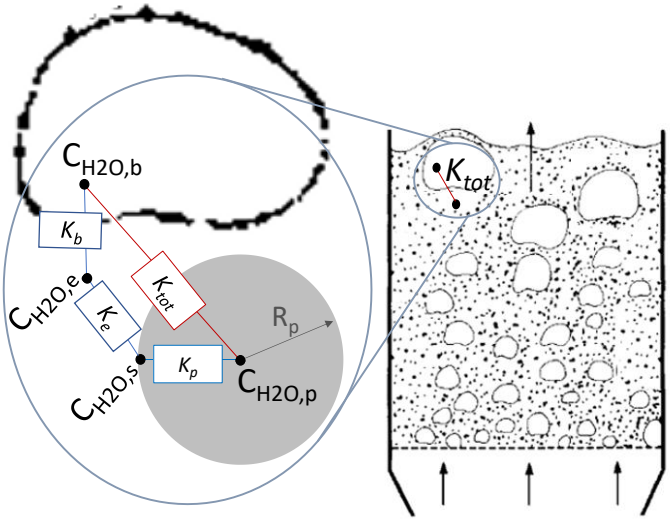

Figure 17. The nature of and relationship of the mass-transfer coefficients, source: Paper V.

The relationship between the coefficients for each of these three contributing mechanisms and the resulting coefficient for the overall mass transfer, K_{tot}, is given by the series-coupling expression given in Table 10.

Table 10. Mass transfer coefficient models presented in Paper V.

Overall mass transfer coefficient (s^{-1})	$\dot{m}(t) = K_{tot} V_R \left(C_{H2O,p} - C_{H2O,b}^{avg}\right)$	(39)
Intra-particle mass transfer coefficient (s^{-1})	$K_P = K_p^* \frac{g(X)}{1-X}$	(40)
where,	$g(X) = 1 - X$	(41)
Mass transfer from particle surface to the emulsion gas (s^{-1})	$Sh = \frac{k_e d_p}{D} = 2\varepsilon_{mf} + 0.7(\frac{Re_{mf}}{\varepsilon_{mf}})^{1/2} Sc^{1/3}$	(42)
where,	$K_e = \frac{k_e A_p}{V_p} = \frac{k_e\, 6}{d_p}$	(43)
Mass transfer from emulsion to the bubbles (s^{-1})	$\frac{1}{K_{tot}} = \frac{1}{K_p} + \frac{1}{K_e} + \frac{1}{K_b}$	(44)

To determine K_p, experimental data obtained from Thermogravimetric analysis (TGA) experiments is used. For K_e, a Frössling-type correlation is selected to describe the mass transfer from particle surface to emulsion gas in the FB. The validity of the Frössling-type correlation is supported by Scala's research on CO oxidation over a Pt catalyst in a BFB [88]. To determine K_{tot}, the two-phase theory of fluidization, as depicted in Figure 18, is considered [18]. Additional details about each step is provided in **Paper V**.

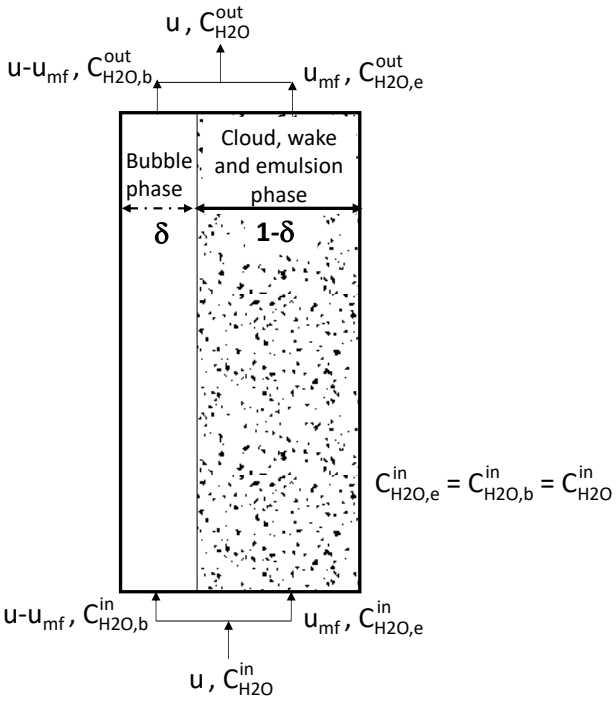

Figure 18. The two-phase theory model of fluidization, source: Paper V.

3.2.3 Dispersion and tank-in-series models

Different models exist to categorize flow patterns based on their proximity to PFR, CSTR, or somewhere in between. In **Papers VI-VII**, the axial dispersion model and the tanks-in-series model are introduced to address deviations from plug flow in reactors. When a diffusion-like process is imposed on plug flow, it is termed axial dispersion or longitudinal dispersion. The axial

dispersion coefficient, D (m²/s), characterizes the extent of this spreading phenomenon. A higher D signifies rapid spreading of the tracer curve, while a lower D indicates slower spreading, and D=0 corresponds to no spreading, representing PFR. The dimensionless group D/uL, known as the vessel dispersion number, quantifies the spread throughout the entire vessel. In the tank-in-series model, it is assumed a number of tanks of the same size are connected in series. Each of these tanks is considered an ideal CSTR unit and represents a distinct portion or segment of the reactor. The number of tanks-in-series can be calculated in different ways. In the present study, the variance of the tracer curve, $\sigma_\theta{}^2$ (-), is employed to extract the information about the quantity of tanks. The models are summarized in Table 11.

Table 11. Vessel dispersion number, tank-in-series and hybrid models.

Vessel dispersion number (-)	$\sigma_\theta{}^2 = \frac{\sigma^2}{\tau^2} = 2\left(\frac{D}{uL}\right) - 2\left(\frac{D}{uL}\right)^2\left[1 - e^{-\frac{uL}{D}}\right]$	(45)
Variance of the tracer curve (s²)	$\sigma^2 = \frac{\int_0^\infty (t-\tau)^2 C_{response,t}\, dt}{\int_0^\infty C_{response,t}\, dt}$	(46)
Mean residence time (s)	$\tau = \frac{\int_0^\infty t C_{response,t}\, dt}{\int_0^\infty C_{response,t}\, dt}$	(47)
Number of tanks (-)	$\sigma_\theta{}^2 = \frac{1}{N}$	(48)
MacMullin and Weber RTD expression	$\tau \times \mathrm{E}_{model} = (\frac{\mathrm{t}}{\tau})^{N-1} \frac{N^N}{(N-1)!} e^{-tN/\tau}$	(49)
Ehybrid-curve model (s⁻¹)	$E_{hybrid} = E_{CSTR} \times E_{PFR} = \int_0^\infty [E_{CSTR}(t') E_{PFR}(t-t')]\, dt'$	(50)

4 Results

The results are categorized into two sections: experimental results and modeling results. This chapter presents and discusses both the experimental findings and the outcomes derived from modeling.

4.1 Fluidization and mapping of pressure drop

Paper I evaluates the effect of different packings on vertical segregation of fluidizing solids. These results are of importance since high segregation will result in less bed material to retain in the packed zone. Therefore, the heat transfer will reduce subsequently in this part of the bed. **Paper I** shows that Hiflow and RMSR packings are much better in retaining bed material in the packed zone up to 13 cm reactor height than the other packings, which suffered from larger tendencies towards vertical segregation at high velocities (Figure 19).

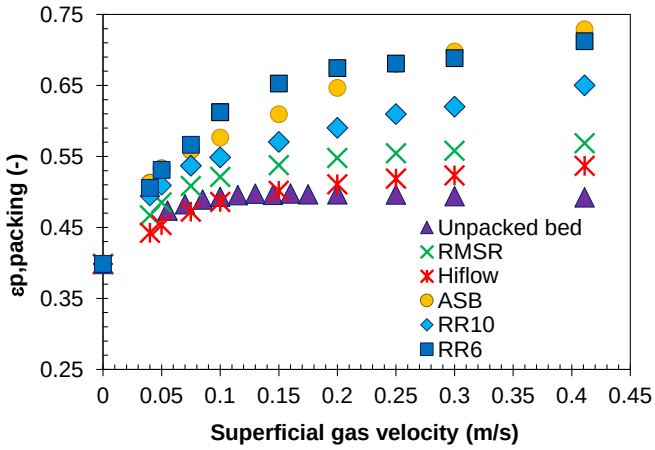

Figure 19. Voidage of fluidizing solids as function of superficial gas velocity for different packings: pressure probe at 13 cm above distributer plate, temperature 800 °C, water flow rate 20 mls^{-1}, stagnant bed packing height 13 cm, source: Paper I.

In **Paper I**, the total pressure drop over the bed (from distributor plate to atmosphere) as function of superficial gas velocity is investigated. All cases with packing show lower pressure drop compared the case with no packings, which can be expected. A reason of this behavior can be that a smaller mass of FB material is present in a packed bed, for a given height, compared to a bed with no packing (Figure 20).

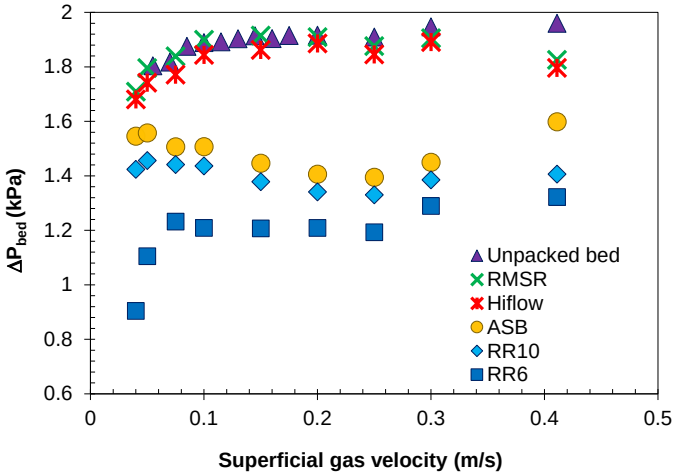

Figure 20. Total pressure drop as function of superficial gas velocity for different packings: temperature 800 °C, water flow rate 20 mls^{-1}, unfluidized bed height 13 cm, source: Paper I.

The pressure drop per mass of fluidizing bed material as function of superficial gas velocity is shown in Figure 21.

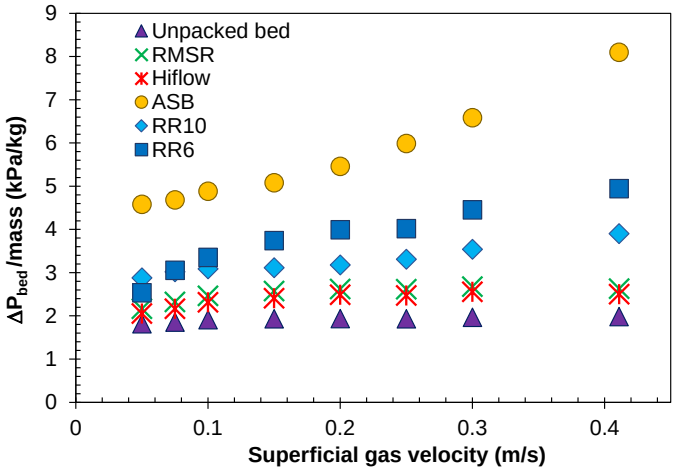

Figure 21. Pressure drop per unit bed mass as function of superficial gas velocity for different packings: differential pressure between the bottom of the bed and the probe located at 13 cm, temperature 800 °C, water flow rate 20 mls^{-1}, initial bed and packing height 13 cm, source: Paper I.

It can be observed that the pressure drop per mass of particles for RMSR and Hiflow packings is approximately constant and rather close to the bed with no packing. It seems clear that these two packings, both of which have very high void factor of >95%, have lower friction between the particles and packings than the other packings. Thus, they behave largely like unpacked beds in this respect. Packings with lower void factor such as RRs and especially the ASB packings, display higher pressure drop per mass of bed material. The main reason should be interaction between fluidization gas, bed particles and packing material, as was outlined in **Paper I**.

4.2 Bed-to-tube heat-transfer

The effect of temperature and superficial gas velocity on bed-to-tube heat transfer coefficient in packed-fluidized beds are investigated in **Paper I**. For the effect of temperature on heat transfer coefficient, results are illustrated at the fixed superficial gas velocity of 0.2 ms^{-1}. Results show that at this superficial gas velocity, heat transfer coefficient varies significantly (671-1298 $Wm^{-2}K^{-1}$) in the temperature range of 400-900 °C (Figure 22).

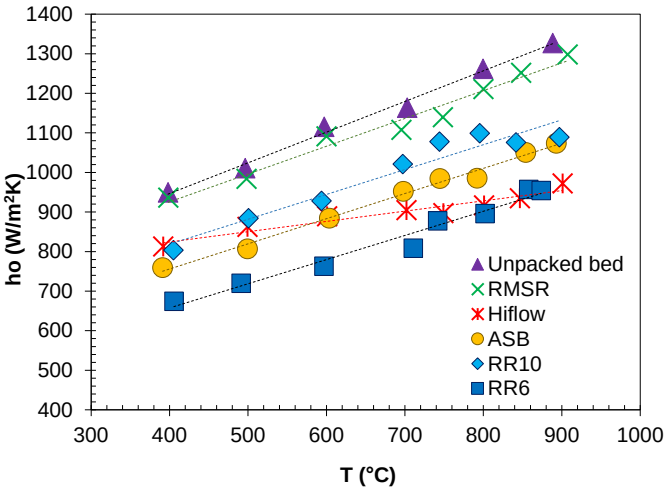

Figure 22. Effect of bed temperature on bed-to-tube heat transfer coefficient in packed-fluidized beds: superficial gas velocity 0.2 ms^{-1}, water flow rate 20 mls^{-1}, stagnant bed and packing height 13 cm, source: Paper I.

At superficial gas velocity of 0.2 ms^{-1}, the bed with no packings showed a higher heat transfer coefficient at all temperatures compared to packed-fluidized beds. However, it can be observed in **Paper I** that RMSR performed essentially equal as the bed with no packings. RR10 displayed the second highest heat transfer coefficients with increasing bed temperature with almost the same trend as ASB. It was showed in **Paper I** that for RR6 heat transfer coefficient decreased compared to RR10. The reason is probably that smaller packings restrict particle movements more and thus decrease heat transfer inside the bed. Since by decreasing the size of RRs from 10 mm to 6 mm, bed restriction and channeling could be expected to intensify. Another finding in **Paper I** was that despite the similar attributes of Hiflow packings to RMSR with respect to nominal size and void factor, the heat transfer when using Hiflow packing was significantly less good than for RMSR packings. This result was discussed in detail in **Paper I**.

The second target of **Paper I** was to evaluate the effect of superficial gas velocity on bed-to-tube heat transfer coefficient. For this purpose, the temperature was kept constant at 800 °C. As described in **Paper I**, at high superficial gas velocities, packed-fluidized bed with RMSR packings shows higher heat transfer coefficient (1243 $Wm^{-2}K^{-1}$) compared to other cases including to the bed without packing, which displayed a maximum heat transfer coefficient of 1124 $Wm^{-2}K^{-1}$ (Figure 23).

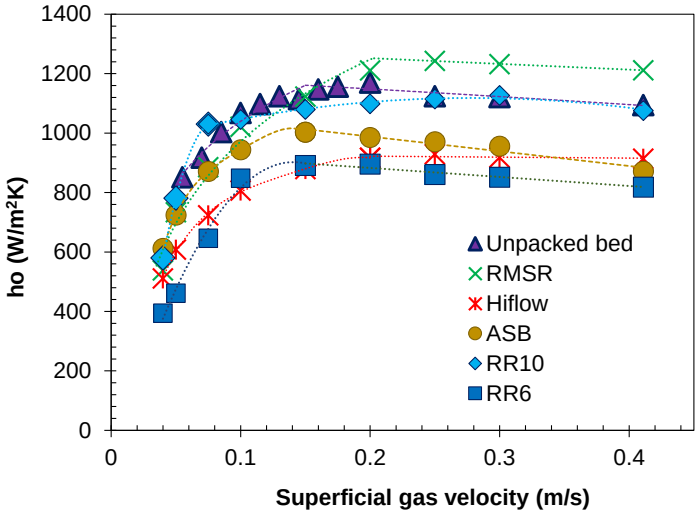

Figure 23. Effect of superficial gas velocity on bed-to-tube heat transfer coefficient in packed-fluidized beds: temperature 800 °C, water flow rate 20 mls^{-1}, stagnant bed height 13 cm, source: Paper I.

The reason for improvements with packings was attributed to their ability to break large bubbles into smaller ones which was further investigated in **Papers II-III**. To facilitate understanding, the behavior of a bed with no packing and increasing gas velocity can be considered. The particulate bed can in this case be divided in two different phases, the emulsion phase and the bubble phase. By increasing gas velocity at a fixed temperature, initially, formation of small bubbles will help increasing the interaction of bed particles with each other and the surface of the water tube. Thus, it will increase heat transfer between bed material and tube. However, increasing gas velocity to higher values will increase the number of bubbles. Eventually, bubbles coalescence will occur and result in formation of bigger bubbles. Since heat transfer is a function mainly of particles coming in direct contact with the tube, this will reduce the heat transfer coefficient. A packing with high void factor such as RMSR, that does not greatly hinder particle movement but breaks down big bubbles to smaller ones, could therefore conceivably improve heat transfer coefficient to a submerged tube, as have been observed in Figure 23.

4.3 Chemical looping combustion in packed-fluidized bed

Based on the findings of **Paper I** on packing's behaviour and their characteristics, different pairs of packings are selected for further investigations in **Papers II-III**. In **Paper II**, RMSR with high void factor (0.96) is compared to ASB with low void factor (0.43). In **Paper III**, the two high void factor packings RMSR (0.96) and Hiflow (0.95) are studied.

General finding in **Papers II-III** is that RMSR shows the most significant improvements. The main reason for better fuel conversion with RMSR packings is attributed to the ability of this packing to increase the mass transfer rate, presumably by breaking down bubbles. At the same time, RMSR packing still allows for similar bed mass for a given volume as an unpacked bed. This is in stark contrast to the ASB packings. Also, the RMSR packings packed more easily in the experimental reactor, as compared to the bulkier Hiflow packings. The average fuel conversion in **Papers II-III** is depicted as function of bed height for the studied packings (Figure 24 and Figure 25).

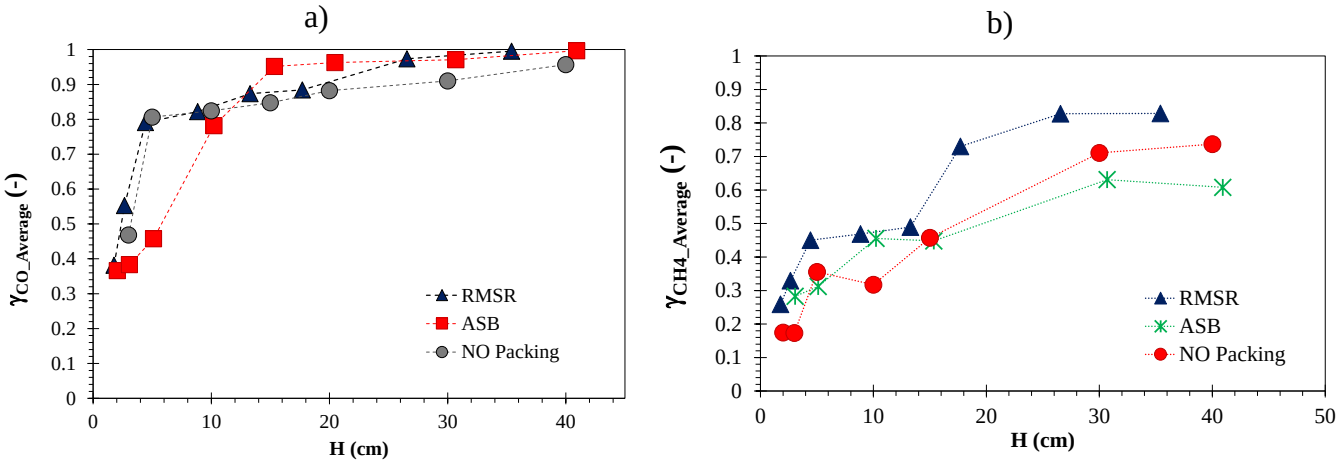

Figure 24. Average fuel conversion as function of bed height, a) CO at 840 °C, b) CH_4 at 940 °C, source: Paper II.

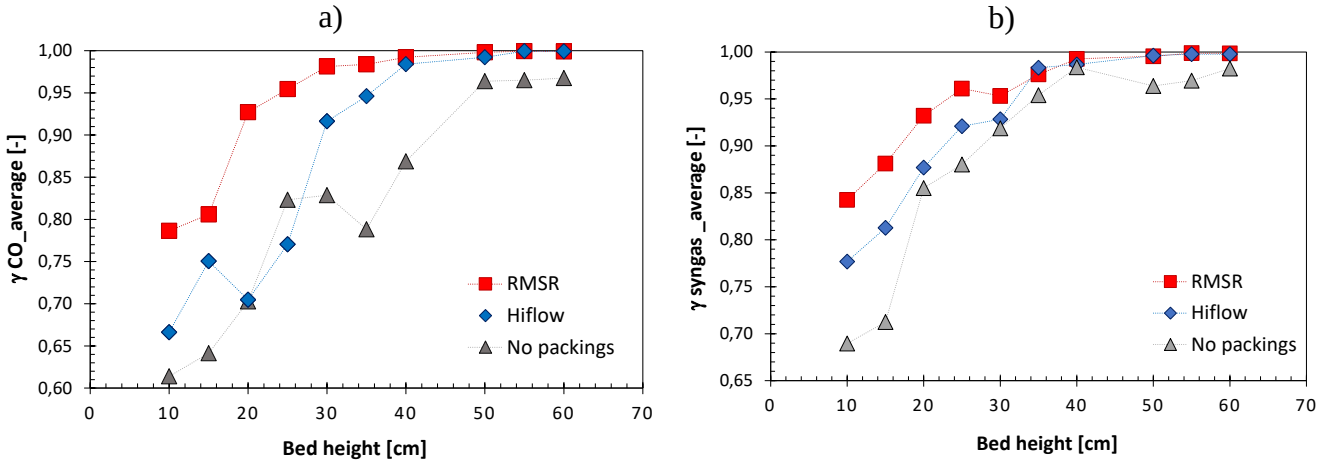

Figure 25. Average fuel conversion as function of bed height, a) CO at 840 °C, b) syngas at 840 °C, source: Paper III.

In **Paper II**, it is shown that with bed depths lower than approximately 15 cm the effect of adding packings is not clear in fuel conversion (Figure 26a). The likely reason is that the packing materials used has the nominal dimensions of 12.7 mm and 25 mm. For low bed heights this means that the packing depth is only a few stacked layers of packing, which may be insufficient to achieve an even flow profile. Also bubble size could be expected to be small with low bed height, leaving limited space for improvement.

In the next step, in **Papers II-III**, average fuel conversion is investigated as a function of pressure drop. **Papers II-III** show that for all the packings studied, there is a significant improvement in fuel conversion for given pressure drop, for the cases which corresponds to deeper bed heights than 5 cm. **Papers II-III** show that the pressure drop for a given conversion of fuels is lower in the packed beds compared to the other alternative without packings (Figure 26 and Figure 27).

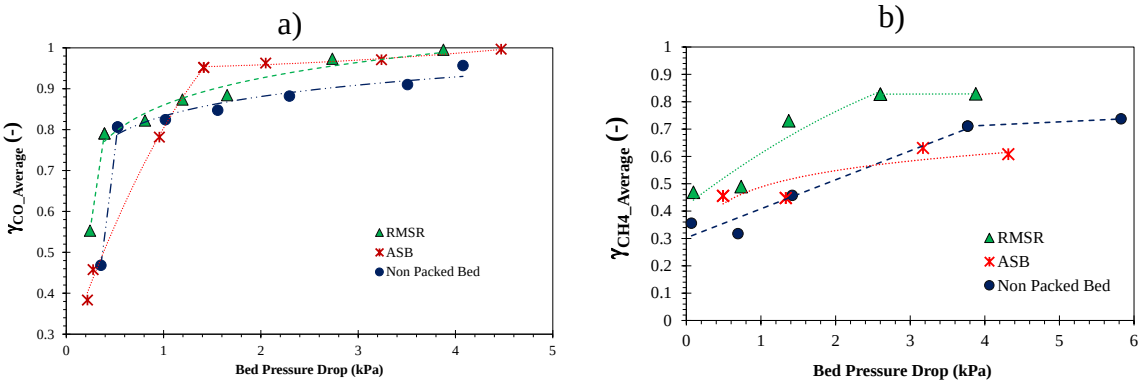

Figure 26. Average fuel conversion as function of bed pressure drop, a) CO at 840 °C, b) CH4 at 940 °C, source: Paper II.

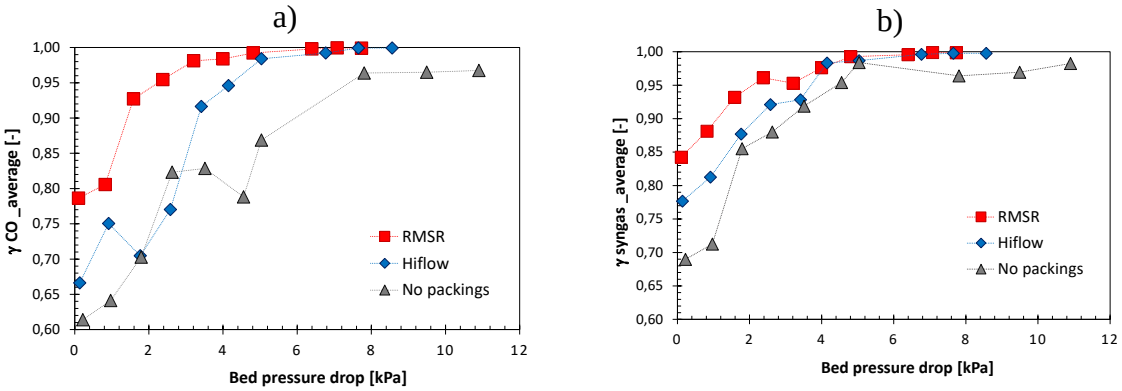

Figure 27. Average fuel conversion as function of bed pressure drop, a) CO at 840 °C, b) syngas at 840 °C, source: Paper III.

4.4 Gas interchange coefficient in packed-fluidized bed

In the last section of **Paper III**, the increased fuel conversion is studied in more depth, and an attempt is made to characterize the mass transfer based on bubble size as well as gas-solid contact efficiency. The behaviour with respect to bubbles is explored through pressure signal data (**Paper III**). This can result in further insights on the effect of packings in the bed. Thus, **Paper III** takes its initial step in investigating bubble size. The average bubble diameter is calculated with equation (38) in Chapter 3. The results are shown in Figure 28.

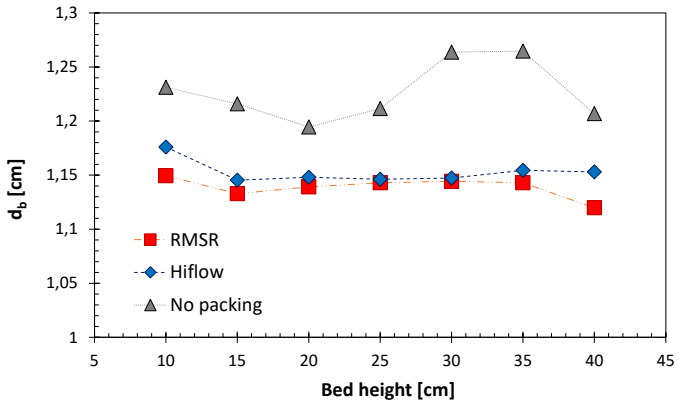

Figure 28. The changes of bubble diameter as function of bed height, as estimated by equation (38): Pressure data gathered and analyzed at MP1 using a measurement frequency of 1 Hz, source: Paper III.

Figure 28 shows the changes of bubble diameter as calculated from the standard deviation of pressure signal data gathered at MP1, located at 3.65 cm above the distributor plate. This measurement point was chosen to assure that for all the bed heights, pressure sensor is inside the bed. Thus, the signals will be related to bubble formation, coalescence, eruption etc. in the packed-fluidized bed and not in the splash zone. The results can be assumed to represent an estimation of an average value (**Paper III**). As discussed in **Paper III**, bubble diameter in packed beds containing high void packings of RMSR and Hiflow are very close to each other and around 8 % less than beds without packings. Thus, the surface area where gas enters or exits the bubble decreases by 17% and the gas volume in each bubble decreases by 25% (Figure 28). It is worth pointing out that bubbles would be expected to grow larger in deeper beds, so for real-world applications of CLC bubble growth could become a very significant issue.

In the final step in **Paper III**, the reaction contact factor, k_f ($Nm^3kg^{-1}s^{-1}$), and gas interchange coefficient, K_{be} (s^{-1}), are calculated with equations (31) and (32) in Chapter 3, respectively. As it is expected that the intrinsic rate constant k_r, in equation (31) would be constant for a certain material, k_f can be seen as an effective contact factor between bed material and gas, and hence a gauge of improved mass-transfer. Results presented in **Paper III** indicate that applying RMSR and Hiflow packings will improve both K_{be} and k_f in the system, compared to a bed with no packings. This improvement is more significant for RMSR packing. This difference in performance between the packings can be due to geometry. For the RMSR packing, more uniform beds with smaller bubbles may be formed and consequently, the improvements are more pronounced than for Hiflow packings. Also, the Hiflow packings are bulkier and this pack less flawlessly in the reactor. Thus, they can be expected to suffer from more significant wall effects. This conclusion is in accordance with **Paper I**, where the heat transfer in the packed- fluidized beds for these packings is investigated.

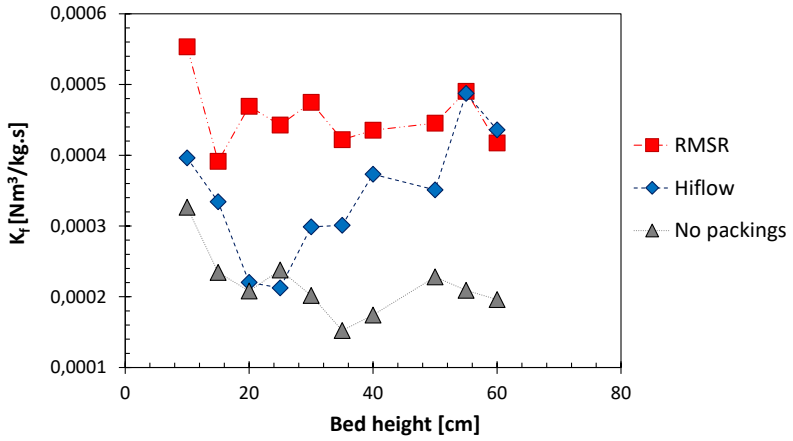

Figure 29. k_f as calculated by equation (31) as a function of bed height, source: Paper III.

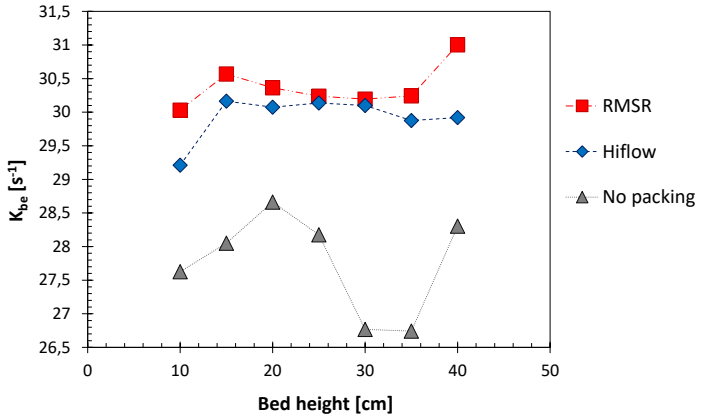

Figure 30. K_{be} as calculated by equation (32) as a function of bed height, source: Paper III.

4.5 Particle to gas mass-transfer

Based on the findings of **Papers II-III** on the fuel gas conversion, a new set of experiments are designed to investigate the impact of random packings in BFBs on the mass-transfer. In **Paper V**, a detailed analysis of the mass transfer is done through a model accounting for the different steps in the mass transfer chain. **Paper V** contributes by both i) coupling experiments with detailed modeling of the important mass-transfer of gas in the FB, ii) applying a new setting of BFBs equipped with random packings.

The absolute humidity at the outlet of the FB under desorption experiments involving 6 kg silica gel and F=2.3 is depicted in Figure 31 for three different cases (no packings and packing of two types). For these experiments, silica gel was first saturated with humidified air holding 12-14 $g_{H2O}/m^3_{dry\ air}$. Then the inlet air was switched from humidified to atmospheric air (here called also dry air) with 0.4 $g_{H2O}/m^3_{dry\ air}$.

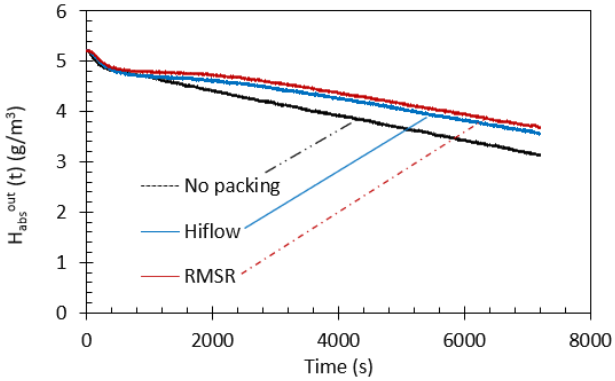

Figure 31. Absolute humidity of the outlet air as a function of time, 6 kg silica gel, F=2.3, source: Paper V.

Regarding the outlet air (as shown in Figure 31), during the initial phase of the experiments (0-1000 s), all three cases exhibited comparable levels of saturation at the experiment's outset. However, in the absence of packing material, a steep decline in outlet humidity occurred shortly thereafter. In contrast, both the RMSR and Hiflow configurations maintained higher outlet absolute humidity levels for an extended duration, persisting until approximately 3000 s. This behavior reflects the higher mass-transfer rate occurring between the silica gel particles and the dry air within the packed-fluidized cases compared to the unpacked bed. Table 12 depicts the resulting amount of desorbed water for the different cases examined.

Table 12. The total value of desorbed water from silica gel particles, source: Paper V.

No.	Packing	Fluidization number (-)	Superficial gas velocity (ms^{-1})	Silica gel (kg)	Amount of desorbed water in 6800 s, Δm_{des} (g)	Improvement compared to No packing (%)
1	No packing	1.7	0.25	4	233.0	-
2	No packing	1.7	0.25	6	242.0	-
3	No packing	1.7	0.25	8	261.0	-
4	No packing	2.3	0.35	4	280.2	-
5	No packing	2.3	0.35	6	308.4	-
6	RMSR	1.7	0.25	4	261.0	12.0
7	RMSR	1.7	0.25	6	276.0	14.0
8	RMSR	1.7	0.25	8	281.0	7.7
9	RMSR	2.3	0.35	4	330.1	17.8
10	RMSR	2.3	0.35	6	361.0	16.9
11	Hiflow	2.3	0.35	6	360.3	16.8

As seen in Table 12, the amount of desorbed water is always larger when packings are applied compared to the unpacked case. This confirms that the presence of packing in the bed improves the mass-transfer compared to a bed with no packing.

4.6 Mass-transfer coefficient in packed-fluidized bed

The values of overall mass transfer coefficient, K_{tot}, the intra-particle mass transfer coefficient K_p, the transfer across the particle surface and the emulsion gas K_e, and the emulsion-to-bubble coefficient, K_b, and presented in Table 13. for the cases investigated. It is important to point out that the emulsion-bubble mass-transfer, is the only parameter that is altered by applying packings.

Table 13. The average value of different mass-transfer coefficients, source: Paper V.

No.	Packing	Fluidization number (-)	Silica gel (kg)	K_b (s^{-1}) (increase %)	K_{tot} (s^{-1})	K_p (s^{-1})	K_e (s^{-1})
1	No packing	1.7	4	9.04e-5	8.84e-5	0.004	803.8
2	No packing	1.7	6	6.25e-5	6.15e-5	0.004	803.8
3	No packing	1.7	8	5.40e-5	5.32e-5	0.004	803.8
4	No packing	2.3	4	8.30e-5	8.13e-5	0.004	803.8
5	No packing	2.3	6	6.21e-5	6.11e-5	0.004	803.8
6	RMSR	1.7	4	10.04e-5 (+15%)	10.14e-5	0.004	803.8
7	RMSR	1.7	6	7.32e-5 (+17%)	7.19e-5	0.004	803.8
8	RMSR	1.7	8	5.60e-5 (+4%)	5.52e-5	0.004	803.8
9	RMSR	2.3	4	9.62e-5 (+16%)	9.39e-5	0.004	803.8
10	RMSR	2.3	6	7.66e-5 (+23%)	7.52e-5	0.004	803.8
11	Hiflow	2.3	6	7.64e-5 (+23%)	7.50e-5	0.004	803.8

As illustrated in Table 13, the overall mass transfer is strongly governed by the emulsion-bubble mass transfer, as indicated by the orders of magnitude of the coefficients for the different steps. The addition of packing materials appears to enhance the emulsion-bubble mass transfer, likely due to the reduction in bubble size and the resultant increase in the interface area between bubbles and the emulsion. It is noteworthy that both types of packings yield an identical increase of 23% in mass transfer for their respective common cases when compared to the unpacked bed condition.

4.7 RTD of solids in packed-fluidized bed

In **Paper IV**, it is demonstrated that using the spherical low-void packings in BFBs has a potential restriction on solids flux, particularly where high solids circulation rates are desired, such as in circulating fluidized bed (CFB) applications like CLC. This restriction is expected, as spherical packings have a low void factor, which hinders solids throughflow. On the other hand, **Paper IV** also shows that the low void packings have potential applications in creating a counter-current flow pattern with respect to gases and solids. This configuration facilitates a progressive decrease in reactant concentration along the reactor length, enhancing the efficiency for reactions where the rate increases with reactant concentration, such as n^{th}-order irreversible reactions or equilibrium reactions, compared to a conventional BFB where concentration drops immediately to a low value inside the reactor. **Papers VI-VII** continue the work initiated in **Paper IV**. These papers investigate the behavior of reactors in achieving plug flow characteristics when packings are applied. In **Papers VI-VII**, a nonreactive tracer is introduced into the reactors via a pulse input method to examine the E-curve. This section provides the results regarding the reactors behavior that can be derived from the analysis of the E-curve data.

4.7.1 Cross-current flow reactor

Figure 32 depicts the E_θ-curve in cross-current flow experiments conducted at a solid throughflow F_s=164 gs^{-1}, fluidization number F=4.4, and settled bed height H=10 cm.

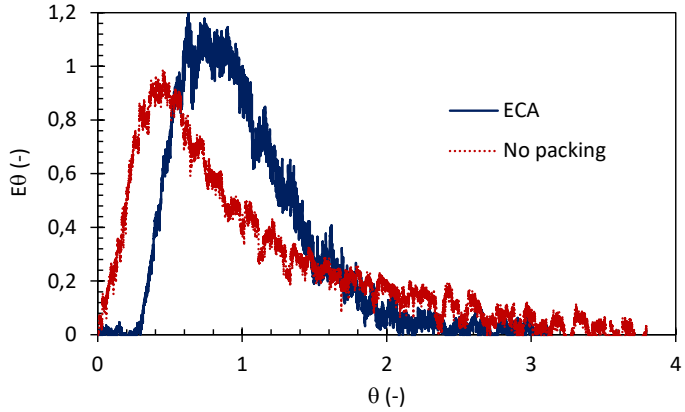

Figure 32. E_θ-curve at the outlet of cross-current BFB: Fs= 164 gs^{-1}, F=4.4, H=10 cm, source: Paper VI.

Comparative analysis of the plots for beds with and without packing, as shown in Figure 32, reveals that the incorporation of packing material narrows the E_θ-curve and shifts its peak towards θ=1. This indicates that the packings reduce horizontal particle mixing in the bed, resulting in a behavior that more closely resembles that of a PFR with axial dispersion. In contrast, the absence of packing material in the system results in behavior that more closely approximates that of a CSTR. Further results are detailed in **Paper VI**. **Paper VI** presents the parameters derived from

cross-current flow experiments utilizing both the dispersion and tank-in-series models. These results are summarized in Table 14 for different solid flow rates, F_s (gs^{-1}), fluidization number, F (-), and packing configurations.

Table 14. Parameters of dispersion and tank-in-series model for cross-current flow, source: Paper VI.

No.	Packing	Air flow	Dispersion model		Tank-in-series model	
	Type	F [-]	D/uL [-]	Pe [-] (variation %)	σ_θ^2 [-]	N [-] (variation %)
	F_s= 92 g/s					
1	No packing	8.8	0.47	2.13 (-)	0.55	1.8 (-)
2	No packing	6.6	0.50	1.99 (-)	0.57	1.8 (-)
3	No packing	4.4	0.48	2.07 (-)	0.56	1.8 (-)
4	ECA	8.8	0.24	4.15 (+94.83)	0.37	2.7 (+49.78)
5	ECA	6.6	0.13	7.61 (+282.57)	0.23	4.4 (+149.33)
6	ECA	4.4	0.11	8.81 (+325.05)	0.20	5.0 (+177.29)
	F_s= 133 g/s					
7	No packing	8.8	0.66	1.50 (-)	0.64	1.6 (-)
8	No packing	6.6	0.48	2.06 (-)	0.56	1.8 (-)
9	No packing	4.4	0.36	2.76 (-)	0.48	2.1 (-)
10	ECA	8.8	0.23	4.31 (+186.53)	0.36	2.8 (+79.47)
11	ECA	6.6	0.15	6.71 (+225.24)	0.25	3.9 (+120.40)
12	ECA	4.4	0.12	8.08 (+192.63)	0.22	4.6 (+120.66)
	F_s= 164 g/s					
13	No packing	8.8	0.42	2.38 (-)	0.52	1.9 (-)
14	No packing	6.6	0.49	2.05 (-)	0.56	1.8 (-)
15	No packing	4.4	0.41	2.47 (-)	0.51	1.9 (-)
16	ECA	8.8	0.14	7.12 (+199.67)	0.24	4.1 (+115.54)
17	ECA	6.6	0.14	7.09 (+246.00)	0.24	4.1 (+131.58)
18	ECA	4.4	0.11	8.99 (+264.28)	0.20	5.1 (+157.89)

The vessel dispersion number, *D/uL* (-), is calculated using equation (45) from Chapter 3. As depicted in Table 14, the utilization of ECA packing consistently results in a decrease in the *D/uL* across all examined scenarios. Consequently, the reactor behavior tends towards resembling a PFR, leading to higher number of theoretical tanks, *N* (-), as indicated by equation (48). A comparison of *N* values between experiments with ECA packing and those with an unpacked bed, reveals that the introduction of packings results in an increase in *N* by up to threefold in comparison to the unpacked beds. Consequently, the reactor's behavior converges towards that of a PFR characterized by higher *N* values and lower *D/uL*.

4.7.2 Counter-current flow reactor

Figure 33 depicts the E_θ-curve in counter-current flow experiments conducted at fluidization number F=15.6, solid throughflow F_s=68 gs^{-1}, and settled bed height H=30 cm.

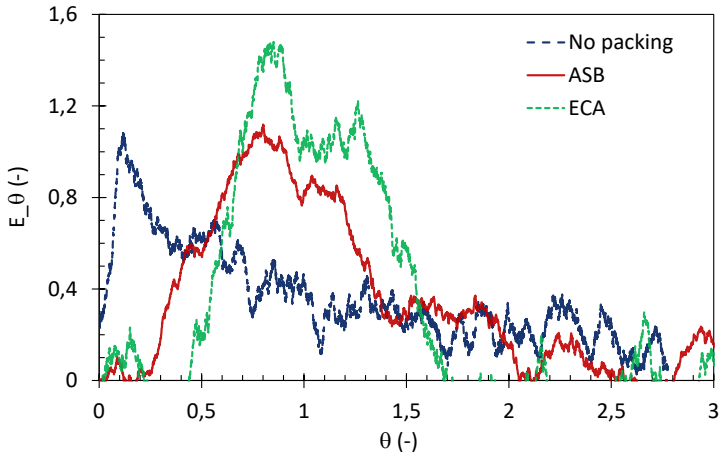

Figure 33. E_θ-curve at the outlet of counter-current BFB: Fs=68 gs^{-1}, F=15.6, H=30 cm, source: Paper VII

A comparative analysis of the plots for beds with and without packing, shown in Figure 33, indicates that the inclusion of ASB and ECA packings make the E_θ-curve narrower and shift the peak towards θ=1. Thus, the packings reduce vertical particle mixing in the reactor, resulting in a behavior more similar to that of a PFR with axial dispersion. In contrast, the absence of packing material aligns the reactor's behavior more closely with that of a CSTR. Further details on the results under different operating conditions are discussed in **Paper VII**.

Paper VII presents the parameters derived from counter-current flow experiments utilizing the dispersion and tank-in-series models. These results are summarized for different fluidization number, *F* (-), bed height, *H* (cm), and packing type in Table 15.

Table 15. Parameters of dispersion and tanks-in-series models for counter-current flow, source: Paper VII.

Packing	Bed inventory	Air flow	Dispersion model		Tank in series model	
Type	H [cm]	F [-]	Pe [-]	D [m^2/s]	σ_θ^2[-]	N [-]
No packing	30	15.6	1.44	0.069	0.65	1
No packing	30	21.9	1.75	0.056	0.65	1
No packing	50	15.6	2.96	0.034	0.46	2
ASB	30	15.6	10.19	0.009	0.17	6
ASB	30	21.9	17.00	0.006	0.11	9
ASB	50	15.6	18.00	0.006	0.10	10
ECA	30	15.6	13.38	0.007	0.14	7

As shown in Table 15, comparing the *N* values between experiments with packings and those with an unpacked bed it is evident that the introduction of packings results in an increase in *N* by up to ninefold compared to the unpacked beds. Consequently, the reactor's behavior converges towards that of a PFR characterized by higher *Pe* and *N* values.

5 Summary and outlook

As discussed in Chapter 2, there have been a limited number of studies on the concept of confined or packed fluidized beds. These studies primarily focus on heat transfer effects, bed expansion, or the hydrodynamic behavior of such packings, with relatively few papers published on the topic. Further, the proposal of many new fluidized bed concepts for sustainable energy conversion in the last decades makes further investigations of packed beds of high interest, as many of these could benefit greatly from enhanced mass and heat transfer and also plug-flow of solids. The main contribution of the thesis is in the comprehensive examination and application of packed-fluidized beds for new energy conversion technologies, like chemical-looping, as explored in **Papers I-VII**. The experiments are conducted at both elevated and ambient temperatures, with the general objective being the utilization of packings to enhance the performance of bubbling fluidized beds (BFB). Void factor is identified as a key characteristic of the packings. Thus, the packings investigated in this thesis can be categorized into two main categories. RMSR and Hiflow are characterized by their high void factor (>95%), while ASB, ECA, and RR have much lower (<58%).

Results of **Papers I-V** show that high void packings have the potential to be applicable to circulating fluidized bed systems such as Chemical Looping Combustion (CLC), due to their potentially low impact on parameters such as solids flux and reactor inventory. Conversely, low void factor packings offer distinct advantages, including the ability to transition the behavior of BFBs from that of a continuous stirred tank reactor (CSTR) to a plug flow reactor (PFR). This transition is explored in **Papers IV, VI,** and **VII**. Some processes that can benefit from PFR reactors, such as FCC and TSA, are already discussed in detail in Chapter 1. Additional examples include the steam-iron reaction and steam methane reforming integrated with CLC for H_2 production [29,30]. Another relevant application is the direct reduction of iron ore using H_2. These reactions are equilibrium reactions. Therefore, conducting them in a PFR would be advantageous in shifting the equilibrium towards the products.

5.1 Discussion

5.1.1 High-void packings

Paper I demonstrates that RMSR packings among the high-void group significantly enhance heat transfer, particularly at higher superficial gas velocities. In contrast, the performance of Hiflow packings is less effective. The reason for this is not totally clear and is discussed in detail in **Paper I**. This may be attributed to the large and bulkier size of these packings which cause it to pack less readily in the small reactors. In fact, the impact on heat transfer by Hiflow packings may be the single most uncertain result in the studies included in this thesis.

The performance difference between RMSR and Hiflow packings is further observed by the fuel conversion studies presented in **Paper III**. Results indicate that RMSR packings have a more favorable geometry for bubble elimination. RMSR may create a tighter lattice structure compared to the more symmetrically shaped Hiflow packings. This tighter structure might be preferable for inhibiting bubbles, leading to more effective bubbling fluidization. Alternatively, it is hypothesized that the bulkier Hiflow packings might not distribute as well in the relatively small reactor vessel used, potentially resulting in unfavorable flow phenomena, such as bypass flow near the reactor wall. However, such phenomena cannot be easily observed in steel reactors. It is worth mentioning that this effect may diminish on a larger scale. Mass transfer experiments detailed in **Paper V**, conducted in a larger setup with an inner diameter of 22 cm, demonstrate that both Hiflow and RMSR packings yield similar improvements in mass transfer.

Given these observations, the selection of packings should be carefully tailored to the specific setup, configuration, and operational conditions. For instance, if one were to consider whether application of high-void packings would be advisable for the 10 kW CLC setup operating at Chalmers University of Technology [82,89] to enhance fuel conversion, the answer would be conditional. Based on the findings here, RMSR packing would be recommended as the first option for the following reasons:

- It is important to note that gas-solid mass transfer is only one of several factors affecting fuel conversion in CLC. The reaction kinetics between the fuel and oxygen carrier is another critical factor, which can vary significantly depending on the specific combinations and process parameters (such as temperature, bed material, and fuel type). Packings will influence fuel conversion only if mass transfer is a significant bottleneck, which appears to be the case for deep beds, as discussed in **Paper II**.
- The fuel reactor in the 10 kW CLC setup is a bubbling fluidized bed with a small cross-section (approximately 234 mm × 85 mm) and a height of around 125 mm. As discussed, RMSR is the most suitable high-void packing for small reactor vessels. It could be integrated into a bubbling fluidized bed with minimal impact on pressure drop and vertical segregation, and without significantly affecting solids throughflow. Additionally, RMSR's ability to reduce bubble size and improve gas-solid mass transfer is expected to be significant, making it a promising option for enhancing CLC performance.
- However, it should be noted that at low bed heights (based on **Papers II-III**), beds with packings exhibit roughly the same fuel conversion as a standard bubbling bed without packings. Therefore, the application of RMSR in the 10 kW CLC should be considered for higher bed heights to effectively improve fuel conversion.
- A critical aspect that is not explored in this thesis is the lifetime and maintenance of packings during continuous CLC operation. Other, uncertainties to consider include the durability of

stainless steel RMSR packings at continuous operation temperatures of 800-900°C, potential alternative materials for corrosive high-temperature environments, the applicability of packings for circulating fluidized beds, and the implications of different fuel feeding systems. For instance, in the 10 kW CLC reactor at Chalmers, the fuel feeding system is top-fed, but what if the feeding system were side-fed? How should the packings be positioned within the reactor to avoid interference with the fuel feeding system, such as a side-wall screw feeder?

Placing the packings within a cage with space from the side walls and feeding system may not be ideal. Additional experiments in **Paper VI** suggest that when packings are confined within a cage, there is a potential for dead zones out of the cage at lower superficial gas velocities. An alternative approach could involve placing a mesh above the feeding system and positioning the packings on top of the mesh, as done in **Paper IV**. Personally, I would recommend the use of a standing mesh above the feeding system.

5.1.2 Low-void packings

The following discussion focuses on the limitations and potential applications of low-void packings. In this context, two semi-spherical low-void packings—aluminum silicate ball (ASB) and expanded clay aggregate (ECA)—are considered. These materials have similar void factors but significantly different densities (ASB: 1390 kg/m³, ECA: 280 kg/m³). In an initial experiment, ECA was found to be fragile and highly vulnerable to attrition/ erosion at elevated velocities, leading to its exclusion from high-temperature experiments. However, the absence of CLC experiments utilizing these packings highlights a gap in the research. It would be valuable to explore their potential for ash adsorption and removal in the fuel reactor during CLC experiments. Given their low density, these packings may float and create a segregated layer on the bed's surface. Similar to high-void packings, they are unlikely to significantly impact pressure drop in the reactor but may influence solid throughflows, as discussed in **Papers VI-VII**. An unanswered question is whether the use of these packings could enhance volatile distribution and ash removal in CLC fuel reactors, such as circulating or bubbling fluidized bed reactors.

Papers I-II investigated the effects of ASB packings on heat transfer and in batch CLC experiments. One critical observation not mentioned in these studies is the cracking and breakage of ASB packings during startup and shutdown due to thermal stresses, a factor that must be considered in pilot-scale or more extensive applications.

Paper IV investigated the impact of applying ASB random packing on solid flux in packed-fluidized beds. The primary objective was to determine the limitations in solids circulation rate when spherical packings were used in circulating fluidized bed applications, such as CLC. The secondary objective was to explore whether packings with a low void factor could create a counter-current flow pattern with respect to gases and solids. This study demonstrates that the use of spherical ASB packings in a fluidized bed significantly impacts solid flux. This result was anticipated, as ASB packings have a low void factor, which hinders flow and fluidization. The measured solid flux ranged from 1.2 to 13.6 $kg \cdot m^{-2} \cdot s^{-1}$, significantly lower than the required solid flux for high-circulation applications like CLC or CLG. For example, Lyngfelt and Leckner [15] suggest a solid flux of 68.8 $kg \cdot m^{-2} \cdot s^{-1}$ in the fuel reactor of CLC. The results of this study indicate that achieving such high solid flux rates is not feasible with spherical packings. For applications requiring high solids circulation, packings with a large void factor that does not hinder solid flux should be preferred.

5.1.3 Implications for new technologies

During the course of this work, an applied research project that seeks to utilize low-void packings to achieve counter-current flow with respect to solids and gases has been initiated. The concept seeks to make use of the unique properties of the packed-fluidized bed concept and apply it for hydrogen production with CO_2 capture via the steam-iron reaction (SIR). In summary, Figure 34 demonstrates a potential application of the concept that involves utilizing high void packings in the fuel reactor (FR) of a CLC process driven by biofuels to produce biochar. Subsequently, the biogenic low-value product gases (CO, CO_2, H_2, CH_4) could be directed to a SIR within the FR, which is equipped with low void spherical packings.

In the FR, iron (III) oxide reduces to iron (II) oxide and/or metallic iron by biomass-derived product gas (mainly CO, H_2, CH_4, CO_2) at 800-1000 °C. Equation (51-53) below are unbalanced net reactions, which in reality takes place in several steps. If FR can establish a counter-current flow of gas and solid metal oxides, it facilitates a shift in the equilibrium toward complete oxidation of the gases.

$$Fe_2O_3(s) + product\ gas \rightarrow Fe_3O_4(s) + CO_2(g) + H_2O\ (g) \quad (51)$$

$$Fe_3O_4(s) + product\ gas \rightarrow FeO(s) + CO_2(g) + H_2O(g) \quad (52)$$

$$FeO(s) + product\ gas \rightarrow Fe(s) + CO_2(g) + H_2O(g) \quad (53)$$

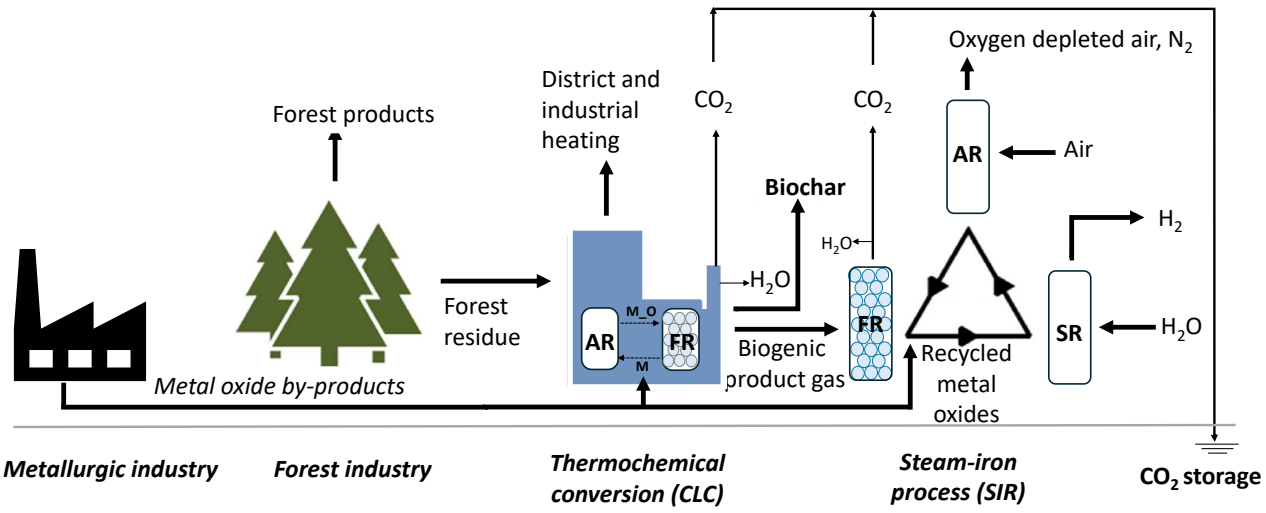

Figure 34. Schematic illustration of the proposed integrated process concept. Biogenic product gas is a weak fuel gas consisting mainly of CO, H_2, CH_4, and CO_2. Metal oxide by-product could be slags or particulate intermediate products rich in iron oxides.

The degree of oxidation of the reducing gas is restricted by the equilibrium [90]. Only reaction (51) is capable of fully oxidizing fuel to CO_2 and H_2O. Reactions (52-53) require significant local partial pressure of H_2 and/or CO and will provide only about 75% conversion of raw product gas. This is a critical point and the reason for why counter-current flow must be realized. The oxidation of iron (II) oxide and/or metallic iron with steam (H_2O) in the steam reactor (SR) at 600-750 °C is also restricted by equilibrium (equation (54-55)). Hence, they can be optimized through the use of counter-current flow.

$$Fe(s) + H_2O\ (g) \rightarrow FeO(s) + H_2\ (g) \quad (54)$$

$$3FeO(s) + H_2O\ (g) \rightarrow Fe_3O_4(s) + H_2\ (g) \quad (55)$$

In the final step within the air reactor (AR), iron (II,III) oxide undergoes oxidation with air at 850-1000 °C (equation 56). This exothermic reaction closes the sequential process loop and enables heat recovery. This step is not necessary unless the production of pure CO_2 is desired.

$$4Fe_3O_4(s) + O_2\ (g) \rightarrow 6Fe_2O_3(s) \quad (56)$$

5.2 Conclusion

This thesis provides a comprehensive investigation of the packed fluidized bed concept. Overall, the results indicate that the technology can provide significant advantages with respect to masss and heat transfer, as well as solid flow patterns, and could thus be instrumental for many new energy technologies, such as chemical-looping. The main conclusions of this work are,

- Packings with high void factor were found to induce limited vertical segregation of bed material. Conversely, the low packing void factor of RR6, RR10, and ASB resulted in a much more noticeable segregation of bed material, especially at high gas velocities (**Paper I**).
- Packings with a high void factor, with RMSR being the best example, can be added to a bubbling fluidized bed with limited effect on heat transfer, pressure drop, and vertical segregation. This is a significant finding since the ability of packings to reduce bubble size and improve gas-solid mass transfer can be expected to be significant. Packings with low void factor, with ASB being the best example, have a much more significant impact on fluidization behaviour (**Paper I, IV**).
- At bed heights lower than 15 cm, beds with different packings had roughly the same fuel conversion as an ordinary bubbling bed without packings in batch CLC reactions (**Paper II**).
- For elevated bed heights (height > 15 cm), fuel conversion improved drastically when packings were used, compared to the corresponding case with no packing (**Papers II-III**). CO conversion >99.5% was achieved with bed height above 30 cm for packed-fluidized bed. With a bed height above 50 cm CO and syngas conversion was essentially 100%. This can be considered as a dramatic improvement, compared to a bubbling bed with no packings. It is believed that was due to improved gas-solid mass transfer, which was achieved by hampering of bubble growth (**Papers II-III**).
- Bubble diameter in packed beds containing high void packings of RMSR and Hiflow is around 8 % less than beds without packings. Thus, the surface area where gas enters or exits the bubble decreases by 17% and the gas volume in each bubble decreases by 25% (**Paper III**).
- Overall, the RMSR packing was found to provide very significant improvement in fuel conversion for all examined fuels. It also has a void factor of 0.96, meaning that it should not influence factors such as solids throughflow or pressure drop greatly. Thus, the use of this sort of packing materials to improve the performance of CLC looks promising (**Papers II-III**).
- In terms of packing size, the results show that the smaller ASB 6.3 mm packing inhibits solid flux more than the larger packings. This is probably because the smaller space in the interstitial voids between these packings does not allow the flow of particles as readily as the larger 12.7 mm ASB (**Paper IV**).

- The desorption of absorbed H_2O from surface of silica particles in a fluidized bed column is mainly controlled by the mass-transfer between the emulsion gas and the bubble phase, which leads to K_b-values within the range $5.4e^{-5}$ – $10.e^{-5}$ s^{-1} and represents almost all of the overall effective mass transfer resistance (**Paper V**).
- The inhibition of bubble formation and growth in the packed-fluidized bed increases the emulsion-bubble mass transfer by up to 23% as compared to the bed without packings. The two types of packing tested (Hiflow and RMSR) yield a similar improvement of the mass transfer (**Paper V**).
- The incorporation of low void packings (ECA and ASB) effectively mitigates particle mixing within a reactor with continuous throughflow of bed material. Consequently, the E-curve in the presence of packings exhibits a closer approximation to a Gaussian shape, indicative of a system behaviour more alike to that of a PFR (**Papers VI-VII**).
- The utilization of low void packings (ECA and ASB) consistently results in a significant increase in the Peclet number (*Pe*). In a cross-current flow reactor, the *Pe* increases by up to four times compared to unpacked configurations (**Paper VI**). In a counter-current flow reactor, this increase can be as much as tenfold (**Paper VII**).
- Analysis using the tank-in-series model indicates a substantial increase in the number of tanks (*N*) for cross-current flow experiments with packing, showing up to a threefold rise compared to unpacked beds. For counter-current flow experiments, this increase is up to ninefold (**Papers VI-VII**).
- Packed fluidized beds could be applicable and promising for a number of new energy technologies where increased mass transfer and plug-flow of solids is an advantage for a well-functioning process, such as chemical-looping, steam-iron and steam-methane hydrogen production, direct reduction of iron ore using H_2, etc.

5.3 Recommendations for further research directions

Based on the key findings of the thesis, several new research directions are suggested:

- All experiments conducted in this work represent fundamental research aimed at demonstrating various aspects of a packed-fluidized bed reactor, based on the type of packing used. It is recommended that future studies focus on scaling up these reactors, or scaling down real reactors that could benefit from specific packed configurations, and investigate the effects of packing in real-world applications.
- The chemical looping combustion (CLC) experiments with high void packings were conducted in a batch CLC reactor. It is advised to perform these experiments in a continuous CLC reactor, examining various parameters such as the lifespan of packings within the reactor. Additionally, comparisons should be made between the performance of packed-fluidized bed operations and operations without packings.
- The packings utilized in this research were commercial products, intended for gases and solids. It is recommended to consider what could be the optimal packings for different applications, and if necessary to focus on the design of specialized packings.
- Previous CLC experiments with biomass have indicated ash-related issues in the fuel reactor due to the alkaline nature of biomass. Future research should aim to identify suitable materials and configurations for packings that can both enhance combustion efficiency in the reactor and selectively capture alkaline materials.

Appendix A– Methane Conversion

This appendix describes the derivation of the momentary conversion equations for CH_4 described in Chapter 3.

Momentary conversion for CH_4 (-)	$X_i = X_{i-1} + \int_{t-1}^{t} \frac{\dot{n} M_O}{m_{ox}} \left(4y_{CO_2} + 3y_{CO} - y_{H_2}\right) dt$	(16)

Equations (A-1)- (A-3) describe the possible reactions between CH_4, oxygen carrier, and the products in the fuel reactor.

(I) $CH_4 + 4M\_O \rightarrow CO_2 + 2H_2O + 4M$ (A-1)

(II) $CH_4 + M\_O \rightarrow CO + 2H_2 + M$ (A-2)

(III) $CO_2 + H_2 \rightarrow CO + H_2O$ (A-3)

For equation (16), the focus lies on the amount of oxygen consumption. The gas analyzer instrument cannot detect water vapor, H_2O, whereas it detects carbon dioxide, CO_2, carbon monoxide, CO, and hydrogen, H_2. To generate 1 molecule of CO_2, 2 oxygen atoms are required (equation A-1). Consequently, the oxygen consumed equals 2 times the quantity of detected CO_2. The same procedure can be followed for CO and H_2O. Thus:

Oxygen consumed:

$$\Delta X = 2y_{CO_{2,out}} + y_{CO,out} + y_{H_2O,out} \quad \text{(A-4)}$$

Carbone balance:

$$y_{CH_{4,in}} = y_{CH_{4,out}} + y_{CO,out} + y_{CO_{2,out}} \quad \text{(A-5)}$$

Hydrogen balance:

$$4y_{CH_{4,in}} = 4y_{CH_{4,out}} + 2y_{H_{2,out}} + 2y_{H_2O,out} \quad \text{(A-6)}$$

or:

$$y_{CH_{4,in}} = y_{CH_{4,out}} + 0.5y_{H_{2,out}} + 0.5y_{H_2O,out} \quad \text{(A-7)}$$

Therefore, by equating the left-hand side of the carbon balance and hydrogen balance equations:

$$y_{CO,out} + y_{CO_{2,out}} = 0.5y_{H_{2,out}} + 0.5y_{H_2O,out} \quad \text{(A-8)}$$

or

$$2y_{CO,out} + 2y_{CO_{2,out}} = y_{H_{2,out}} + y_{H_2O,out} \quad \text{(A-9)}$$

Thus:

$$y_{H_2O,out} = 2y_{CO,out} + 2y_{CO_{2,out}} - y_{H_{2,out}} \quad \text{(A-10)}$$

Replacing equation (A-10) within equation (A-4) gives:

Oxygen consumed:

$$\Delta X = 2y_{CO_{2,out}} + y_{CO,out} + 2y_{CO,out} + 2y_{CO_{2,out}} - y_{H_{2,out}} \quad \text{(A-11)}$$

or:

$$\Delta X = 4y_{CO_{2,out}} + 3y_{CO,out} - y_{H_{2,out}} \quad \text{(A-12)}$$

Appendix B– Syngas Conversion

This appendix describes the derivation of the momentary conversion equations for Syngas (50% CO, 50% H_2) described in Chapter 3.

Momentary conversion for syngas (-) $X_i = X_{i-1} + \int_{t-1}^{t} \frac{\dot{n} M_O}{m_{ox}} \left(2y_{CO_2} + y_{CO} - y_{H_2}\right) dt$ (17)

The possible reactions between Syngas and oxygen carrier in the fuel reactor are:

(I) $CO + M\_O \rightarrow CO_2 + M$ (B-1)

(II) $H_2 + M\_O \rightarrow H_2O + M$ (B-2)

Oxygen consumed:

$\Delta X = y_{CO_{2,out}} + y_{H_2O,out}$ (B-3)

Carbone balance:

$y_{CO,\text{in}} = y_{CO,out} + y_{CO_{2,out}}$ (B-4)

Hydrogen balance:

$y_{H_{2,\text{in}}} = y_{H_{2,out}} + y_{H_2O,out}$ (B-5)

Remember that:

$y_{CO,\text{in}} = y_{H_{2,\text{in}}}$ (B-6)

Thus:

$y_{CO,out} + y_{CO_{2,out}} = y_{H_{2,out}} + y_{H_2O,out}$ (B-7)

or:

$y_{H_2O,out} = y_{CO,out} + y_{CO_{2,out}} + y_{H_{2,out}}$ (B-8)

Oxygen consumed:

$\Delta X = y_{CO_{2,out}} + y_{CO,out} + y_{CO_{2,out}} + y_{H_{2,out}}$ (B-9)

or:

$\Delta X = 2y_{CO_{2,out}} + y_{CO,out} + y_{H_{2,out}}$ (B-10)

References

[1] United Nations. Take Action for the Sustainable Development Goals. Https://WwwUnOrg/Sustainabledevelopment/Sustainable-Development-Goals/ 2024.

[2] Rueda O, Mogollón JM, Tukker A, Scherer L. Negative-emissions technology portfolios to meet the 1.5 °C target. Global Environmental Change 2021;67:102238. https://doi.org/10.1016/j.gloenvcha.2021.102238.

[3] Fuss S, Canadell JG, Peters GP, Tavoni M, Andrew RM, Ciais P, et al. Betting on negative emissions. Nature Climate Change 2014;4:850–3.

[4] Bui M, Adjiman CS, Bardow A, Anthony EJ, Boston A, Brown S, et al. Carbon capture and storage (CCS): the way forward. Energy & Environmental Science 2018;11:1062–176.

[5] Al-Fattah SSM, Barghouty MF, Gaella Bureau BOD, Fillacier S, Thiez PL, McQuale C, et al. Carbon Capture and Storage : Technologies, Policies, Economics, and Implementation Strategies. 1st ed. Taylor Francis Group; 2011.

[6] Lyngfelt A, Rydén M. Negative CO2 Emissions with Chemical-Looping Combustion of Biomass. 2018.

[7] Tong A, Bayham S, Kathe M V., Zeng L, Luo S, Fan L-S. Iron-based syngas chemical looping process and coal-direct chemical looping process development at Ohio State University. Appl Energy 2014;113:1836–45. https://doi.org/10.1016/j.apenergy.2013.05.024.

[8] Mendiara T, Gayán P, García-Labiano F, de Diego LF, Pérez-Astray A, Izquierdo MT, et al. Chemical Looping Combustion of Biomass: An Approach to BECCS. Energy Procedia 2017;114:6021–9. https://doi.org/10.1016/j.egypro.2017.03.1737.

[9] Mei D, Mendiara T, Abad A, de Diego LF, García-Labiano F, Gayán P, et al. Evaluation of Manganese Minerals for Chemical Looping Combustion. Energy & Fuels 2015;29:6605–15. https://doi.org/10.1021/acs.energyfuels.5b01293.

[10] Lyngfelt A, Brink A, Langørgen Ø, Mattisson T, Rydén M, Linderholm C. 11,000 h of chemical-looping combustion operation—Where are we and where do we want to go? International Journal of Greenhouse Gas Control 2019;88:38–56. https://doi.org/10.1016/j.ijggc.2019.05.023.

[11] Jerndal E, Mattisson T, Lyngfelt A. Thermal Analysis of Chemical-Looping Combustion. Chemical Engineering Research and Design 2006;84:795–806. https://doi.org/10.1205/cherd05020.

[12] Adánez J, Abad A, Mendiara T, Gayán P, de Diego LF, García-Labiano F. Chemical looping combustion of solid fuels. Prog Energy Combust Sci 2018;65:6–66. https://doi.org/10.1016/j.pecs.2017.07.005.

[13] Lyngfelt A. Chemical-looping combustion of solid fuels – Status of development. Appl Energy 2014;113:1869–73. https://doi.org/10.1016/j.apenergy.2013.05.043.

[14] Lyngfelt A, Pallarès D, Linderholm C, Lind F, Thunman H, Leckner B. Achieving Adequate Circulation in Chemical Looping Combustion─Design Proposal for a 200 MW th Chemical Looping Combustion Circulating Fluidized Bed Boiler. Energy & Fuels 2022;36:9588–615. https://doi.org/10.1021/acs.energyfuels.1c03615.

[15] Lyngfelt A, Leckner B. A 1000 MWth boiler for chemical-looping combustion of solid fuels – Discussion of design and costs. Appl Energy 2015;157:475–87. https://doi.org/10.1016/j.apenergy.2015.04.057.

[16] Samprón I, Purnomo V, Mattisson T, Leion H, de Diego LF, García-Labiano F. Catalytic Activity of Oxygen Carriers on the Removal of Tar Byproducts for Biomass Chemical Looping Gasification Application. Energy & Fuels 2023;37:16629–38. https://doi.org/10.1021/acs.energyfuels.3c02750.

[17] Rydén M, Lyngfelt A, Mattisson T. Synthesis gas generation by chemical-looping reforming in a continuously operating laboratory reactor. Fuel 2006;85:1631–41. https://doi.org/10.1016/j.fuel.2006.02.004.

[18] Kunii DO, Levenspiel. Fluidization engineering. 2nd ed. Newton, MA, USA: Butterworth-Heinemann; 1991.

[19] Johnsson JE, Grace JR, Graham JJ. Fluidized-Bed Reactor Model Verification on a Reactor of Industrial Scale. AIChE 1987;33:619–27.

[20] Uraz C, Atalay S. Oxidation of Benzene to Maleic Anhydride in a Fluidized Bed Reactor. Chem Eng Technol 2007;30:1708–15.

[21] Westerink EJ, Westerterp KR. Stable Design and Operation of Catalytic Fluidized-Bed Reactors for Multiple Reactions: Uniqueness and Multiplicity. Chem Eng Sci 1990;45:317–32.

[22] Levenspiel O. Chemical Reaction Engineering. vol. 38. 1999.

[23] Levenspiel O. Tracer Technology. vol. 96. New York, NY: Springer New York; 2012. https://doi.org/10.1007/978-1-4419-8074-8.

[24] Rall RR. Apparatus for Contacting of Gases and Solids in Fluidized Bed. US 6,224,833 B1, 2001.

[25] Senegas, M.A.; Patureaux, T.; Selem, P.; Mauleon JL; Process and apparatus for stripping fluidized solids and use thereof in a fluid cracking process. US Patent 5716585, 1998.

[26] Pröll T, Schöny G, Sprachmann G, Hofbauer H. Introduction and evaluation of a double loop staged fluidized bed system for post-combustion CO 2 capture using solid sorbents in a continuous temperature swing adsorption process. Chem Eng Sci 2016;141:166–74. https://doi.org/10.1016/j.ces.2015.11.005.

[27] Pirklbauer J, Schöny G, Zerobin F, Pröll T, Hofbauer H. Optimization of Stage Numbers in a Multistage Fluidized Bed Temperature Swing Adsorption System for CO2 Capture. Energy Procedia 2017;114:2173–81. https://doi.org/10.1016/j.egypro.2017.03.1354.

[28] Eder C. Solids mixing and wall-to-bed heat transfer in cross-flow bubbling fluidized bed reactors with different immersed tube bundles. University of Natural Resources and Life Science, Vienna, 2021.

[29] Rydén M, Lyngfelt A. Using steam reforming to produce hydrogen with carbon dioxide capture by chemical-looping combustion. Int J Hydrogen Energy 2006;31:1271–83. https://doi.org/10.1016/j.ijhydene.2005.12.003.

[30] Stenberg V, Rydén M, Mattisson T, Lyngfelt A. Exploring novel hydrogen production processes by integration of steam methane reforming with chemical-looping combustion (CLC-SMR) and oxygen carrier aided combustion (OCAC-SMR). International Journal of Greenhouse Gas Control 2018;74:28–39. https://doi.org/10.1016/j.ijggc.2018.01.008.

[31] Mei D, Linderholm C, Lyngfelt A. Performance of an oxy-polishing step in the 100 kWth chemical looping combustion prototype. Chemical Engineering Journal 2021;409:128202. https://doi.org/10.1016/j.cej.2020.128202.

[32] Hofer G, Märzinger T, Eder C, Pröll F, Pröll T. Particle mixing in bubbling fluidized bed reactors with continuous particle exchange. Chem Eng Sci 2019;195:585–97. https://doi.org/10.1016/j.ces.2018.10.001.

[33] Bachmann P, Bück A, Tsotsas E. Experimental investigation and correlation of the Bodenstein number in horizontal fluidized beds with internal baffles. Powder Technol 2017;308:378–87. https://doi.org/10.1016/j.powtec.2016.11.025.

[34] Eder C, Hofer G, Beer J, Pröll T. Particle Mixing in Bubbling Fluidized Bed Reactors with Immersed Heat Exchangers and Continuous Particle Exchange. Ind Eng Chem Res 2020;59:19736–50. https://doi.org/10.1021/acs.iecr.0c03568.

[35] Kong W, Wang B, Baeyens J, Li S, Ke H, Tan T, et al. Solids mixing in a shallow cross-flow bubbling fluidized bed. Chem Eng Sci 2018;187:213–22. https://doi.org/10.1016/j.ces.2018.04.073.

[36] Zhou Q, Zeng L, Fan L. Syngas chemical looping process: Dynamic modeling of a moving-bed reducer. AIChE Journal 2013;59:3432–43. https://doi.org/10.1002/aic.14181.

[37] Hsieh T-L, Zhang Y, Xu D, Wang C, Pickarts M, Chung C, et al. Chemical Looping Gasification for Producing High Purity, H 2 -Rich Syngas in a Cocurrent Moving Bed Reducer with Coal and Methane Cofeeds. Ind Eng Chem Res 2018;57:2461–75. https://doi.org/10.1021/acs.iecr.7b04204.

[38] Aronsson J, Krymarys E, Stenberg V, Mattisson T, Lyngfelt A, Rydén M. Improved Gas–Solids Mass Transfer in Fluidized Beds: Confined Fluidization in Chemical-Looping Combustion. Energy & Fuels 2019;33:4442–53. https://doi.org/10.1021/acs.energyfuels.9b00508.

[39] Merrett KM, Whitty KJ. Conversion of Coal in a Fluidized Bed Chemical Looping Combustion Reactor with and without Oxygen Uncoupling. Energy & Fuels 2019;33:1547–55. https://doi.org/10.1021/acs.energyfuels.8b03581.

[40] Song X, Wang Z, Jin Y, Tanaka Z. Gas-solids circulating fluidization in a packed bed. Powder Technol 1995;83:127–31. https://doi.org/10.1016/0032-5910(94)02948-N.

[41] Sutherland JP, Vassilatos G, Kubota H, Osberg GL. The effect of packing on a fluidized bed. AIChE Journal 1963;9:437–41. https://doi.org/10.1002/aic.690090406.

[42] Kang WK, Sutherland JP,, Osberg GL,. Pressure fluctuations in a fluidized bed with and without screen cylindrical packings. Industrial & Engineering Chemistry Fundamentals 1967;6:499–504.

[43] Aronsson J, Pallarès D, Rydén M, Lyngfelt A. Increasing Gas–Solids Mass Transfer in Fluidized Beds by Application of Confined Fluidization—A Feasibility Study. Applied Sciences 2019;9:634. https://doi.org/10.3390/app9040634.

[44] Verver AB, van Swaaij WPM. The heat-transfer performance of gas—solid trickle flow over a regularly stacked packing. Powder Technol 1986;45:133–44. https://doi.org/10.1016/0032-5910(66)80005-0.

[45] Nemati N, Andersson P, Stenberg V, Rydén M. Experimental Investigation of the Effect of Random Packings on Heat Transfer and Particle Segregation in Packed-Fluidized Bed. Ind Eng Chem Res 2021;60:10365–75. https://doi.org/10.1021/acs.iecr.1c01221.

[46] Mandal D, Sathiyamoorthy D, Vinjamur M. Heat Transfer Characteristics of Lithium Titanate Particles in Gas-Solid Packed Fluidized Beds. Fusion Science and Technology 2012;62:150–6. https://doi.org/10.13182/FST12-A14128.

[47] Roes AWM, Van Swaaij WPM. Axial dispersion of gas and solid phases in a gas—solid packed column at trickle flow. The Chemical Engineering Journal 1979;18:13–28. https://doi.org/10.1016/0300-9467(79)80010-6.

[48] Donsì G, Ferrari G, Formisani B. Expansion behaviour of confined fluidized beds of fine particles. Can J Chem Eng 1989;67:185–90. https://doi.org/10.1002/cjce.5450670204.

[49] Girimonte R, Vivacqua V. The expansion process of particle beds fluidized in the voids of a packing of coarse spheres. Powder Technol 2011;213:63–9. https://doi.org/10.1016/j.powtec.2011.07.006.

[50] Claus G, Vergnes F, Goff P Le. Hydrodynamic study of gas and solid flow through a screen-packing. Can J Chem Eng 1976;54:143–7. https://doi.org/10.1002/cjce.5450540304.

[51] Gabor JD, Mecham WJ. Engineering Development of Fluid-Bed Fluoride Volatility Processes, Part 4. Fluidized-packed Beds: Studies of Heat Transfer, Solid gas mixing, and Elutriation. AEC Research and Development Report. 45th ed., Chemical Separation Processes for Plutonium and Uranium; 1965, p. 1–127.

[52] Echigoya E, Osberg GL. Oxidation of ethylene using silver catalyst coated strips in an inert fluidized bed. Can J Chem Eng 1960;38:108–12. https://doi.org/10.1002/cjce.5450380404.

[53] McIlhinney AE, Osberg GL. Silver sprayed cylindrical mesh packing in a fluidized bed. Can J Chem Eng 1964;42:232–3. https://doi.org/10.1002/cjce.5450420511.

[54] Ishii T, Osberg GL. Effect of packing on the catalytic isomerization of cyclopropane in fixed and fluidized beds. AIChE Journal 1965;11:279–87. https://doi.org/10.1002/aic.690110219.

[55] Farrell RJ, Ziegler EN. Kinetics and mass transfer in a fluidized packed-bed: Catalytic hydrogenation of ethylene. AIChE Journal 1979;25:447–55. https://doi.org/10.1002/aic.690250309.

[56] Buczek B, Zabierowski P. Confined fluidization of fines in fixed bed of coarse particles. Chemical and Process Engineering 2016;37:545–57. https://doi.org/10.1515/cpe-2016-0044.

[57] Girimonte R, Formisani B, Testa F. Adsorption of CO2 on a confined fluidized bed of pelletized 13X zeolite. Powder Technol 2017;311:9–17. https://doi.org/10.1016/j.powtec.2017.01.033.

[58] Girimonte R, Formisani B, Testa F. CO2 adsorption in a confined fluidized bed of zeolite pellets: Influence of operating velocity. Particuology 2019;46:67–74. https://doi.org/10.1016/j.partic.2018.08.004.

[59] Gabor JD, Mecham WJ. Radial gas mixing in fluidized-packed beds. . Industrial & Engineering Chemistry Fundamentals 1964;3:60–5.

[60] Gabor JD. Lateral solids mixing in fludized-packed beds. AIChE Journal 1964;10:345–50. https://doi.org/10.1002/aic.690100313.

[61] Gabor JD. Lateral transport in a fluidized-packed bed: Part I. Solids mixing. AIChE Journal 1965;11:127–9. https://doi.org/10.1002/aic.690110126.

[62] Gabor JD, Stangeland BE, Mecham WJ. Lateral transport in a fluidized-packed bed: Part II. Heat transfer. AIChE Journal 1965;11:130–2. https://doi.org/10.1002/aic.690110127.

[63] Anastasia LJ, Gabor JD, Mecham WJ. Engineering Development of Fluid-Bed Fluoride Volatility Processes. Part 3. Fluid-Bed Fluorination of Uranium Dioxide Fuel Pellets. 1965.

[64] Roes AWM, van Swaaij WPM. Hydrodynamic behaviour of a gas—solid counter-current packed column at trickle flow. The Chemical Engineering Journal 1979;17:81–9. https://doi.org/10.1016/0300-9467(79)85001-7.

[65] Roes AWM, van Swaaij WPM. Mass transfer in a gas—solid packed column at trickle flow. The Chemical Engineering Journal 1979;18:29–37. https://doi.org/10.1016/0300-9467(79)80011-8.

[66] Westerterp KR, Kuczynski M. Gas-solid trickle flow hydrodynamics in a packed column. Chem Eng Sci 1987;42:1539–51. https://doi.org/10.1016/0009-2509(87)80159-8.

[67] Donsì G, Ferrari G, Formisani B, Longo G. Confined fluidization of fine particles in a packed bed of coarse particles: Model and experimental description. Powder Technol 1990;61:75–85. https://doi.org/10.1016/0032-5910(90)80068-A.

[68] Ziółkowski D, Michalski J. Onset of fluidization of fines in an organized system within voids of packings formed of spherical elements. Chem Eng Sci 1992;47:4007–16. https://doi.org/10.1016/0009-2509(92)85150-A.

[69] van der Ham AGJ, Prins W, van Swaaij WPM. A small-scale regularly packed circulating fluidized bed. Powder Technol 1994;79:17–28. https://doi.org/10.1016/0032-5910(93)02805-K.

[70] Nikačević NM, Duduković AP. Fluid dynamics of gas-flowing solids-fixed bed contactors. Chemical Industry and Chemical Engineering Quarterly/CICEQ 2007;13:151–62.

[71] Nikačević NM, Predojević ZJ, Petrović DLj, Duduković A. Static holdup in Gas – Flowing solids – Fixed bed contactors. Powder Technol 2009;191:122–9. https://doi.org/10.1016/j.powtec.2008.09.011.

[72] Girimonte R, Vivacqua V. Design criteria for homogeneous fluidization of Geldart's class b solids upward through a packed bed. Powder Technol 2013;249:316–22. https://doi.org/10.1016/j.powtec.2013.08.041.

[73] Davydov L, Spieker WA, Palmas P. COUNTER-CURRENT FLUIDIZED BED REACTOR FOR THE DEHYDROGENATION OF OLEFINS. 9,150,466 B2, 2015.

[74] Girimonte R, Vivacqua V, Formisani B. Extension of the model of binary fluidization to beds confined in a packing of coarse spheres. Powder Technol 2016;297:275–82. https://doi.org/10.1016/j.powtec.2016.04.034.

[75] Guo X, Sun Y, Li R, Yang F. Experimental investigations on temperature variation and inhomogeneity in a packed bed CLC reactor of large particles and low aspect ratio. Chem Eng Sci 2014;107:266–76. https://doi.org/10.1016/j.ces.2013.12.032.

[76] Piovano S, Salierno GL, Montmany E, D'Agostino M, Maestri M, Cassanello M. Bed Expansion and Particle Classification in Liquid Fluidized Beds with Structured Internals. Chem Eng Technol 2015;38:423–30. https://doi.org/10.1002/ceat.201400463.

[77] Zhao G, Shi X, Wu Y, Wang M, Zhang M, Gao J, et al. 3D CFD simulation of gas-solids hydrodynamics and bubbles behaviors in empty and packed bubbling fluidized beds. Powder Technol 2019;351:1–15. https://doi.org/10.1016/j.powtec.2019.04.003.

[78] Maurer S, Gschwend D, Wagner EC, Schildhauer TJ, Ruud van Ommen J, Biollaz SMA, et al. Correlating bubble size and velocity distribution in bubbling fluidized bed based on X-ray tomography. Chemical Engineering Journal 2016;298:17–25. https://doi.org/10.1016/j.cej.2016.02.012.

[79] Maurer S, Schildhauer TJ, Ruud van Ommen J, Biollaz SMA, Wokaun A. Scale-up of fluidized beds with vertical internals: Studying the sectoral approach by means of optical probes. Chemical Engineering Journal 2014;252:131–40. https://doi.org/10.1016/j.cej.2014.04.083.

[80] Maurer S, Wagner EC, Schildhauer TJ, van Ommen JR, Biollaz SMA, Mudde RF. X-ray measurements of bubble hold-up in fluidized beds with and without vertical internals. International Journal of Multiphase Flow 2015;74:118–24. https://doi.org/10.1016/j.ijmultiphaseflow.2015.03.009.

[81] Rydén M, Arjmand M. Continuous hydrogen production via the steam–iron reaction by chemical looping in a circulating fluidized-bed reactor. Int J Hydrogen Energy 2012;37:4843–54. https://doi.org/10.1016/j.ijhydene.2011.12.037.

[82] Moldenhauer P, Rydén M, Mattisson T, Jamal A, Lyngfelt A. Chemical-looping combustion with heavy liquid fuels in a 10 kW pilot plant. Fuel Processing Technology 2017;156:124–37. https://doi.org/10.1016/j.fuproc.2016.10.027.

[83] Stenberg V, Rydén M, Mattisson T, Lyngfelt A. Experimental Investigation of Oxygen Carrier Aided Combustion (OCAC) with Methane and PSA Off-Gas. Applied Sciences 2020;11:210. https://doi.org/10.3390/app11010210.

[84] Sinnott RK, J.M.C., Richardson JF. Coulson & Richardson's Chemical Engineering. vol. 6. 2005.

[85] F. Incropera F, T. Bergman T, Lavine A. Principles of Heat and Mass Transfer. Singapore: 2013.

[86] Welty J, Wicks C, Wilson R, Rorrer G. Fundamentals of Momentum, Heat and Mass Transfer. USA, Wiley: Hoboken, N.J.; 2005.

[87] Hofer G, Schöny G, Pröll T. Acting on hydrodynamics to improve the local bed-to-wall heat transfer in bubbling fluidized beds. Chemical Engineering Research and Design 2018;134:309–18. https://doi.org/10.1016/j.cherd.2018.04.015.

[88] Scala F. Mass transfer around freely moving active particles in the dense phase of a gas fluidized bed of inert particles. Chem Eng Sci 2007;62:4159–76. https://doi.org/10.1016/j.ces.2007.04.040.

[89] Schmitz M, Linderholm C. Chemical looping combustion of biomass in 10- and 100-kW pilots – Analysis of conversion and lifetime using a sintered manganese ore. Fuel 2018;231:73–84. https://doi.org/10.1016/j.fuel.2018.05.071.

[90] Voitic G, Hacker V. Recent advancements in chemical looping water splitting for the production of hydrogen. RSC Adv 2016;6:98267–96. https://doi.org/10.1039/C6RA21180A.